DRAG- LINE SENSOR FOR DRONE ASSISTED METEORITE DETECTION.

Dominic Su

Bachelor of Engineering
Mechatronics Engineering Major

Department of Electronic Engineering
Macquarie University

November 6 2017

Supervisor: Dr. David Inglis

ACKNOWLEDGMENTS

I would like to acknowledge and thank my supervisor Dr. David Inglis for his guidance and support though feedback and mind opening discussions. His support in both his knowledge and advice on academic writing has proved invaluable. I would also like to thank Dr Craig O'Neill for lending me the sensors and meteorite sample. Without them this project would not of been possible. Lastly i would like to thank for family for putting up with my antisocial behaviour whilst finishing off this thesis.

STATEMENT OF CANDIDATE

I, Dominic Su, declare that this report, submitted as part of the requirement for the award of Bachelor of Engineering in the Department of Mechatronics Engineering, Macquarie University, is entirely my own work unless otherwise referenced or acknowledged. This document has not been submitted for qualification or assessment at any academic institution.

Student's Name: Dominic Su

Student's Signature: Dominic Su

Date: 06/11/2017

ABSTRACT

Meteorites are great scientific materials in the study of astronomy, planetary geology and astrobiology. They not only provide a glimpse into the wider cosmos but also stimulate research into the respective fields (as stated above), due to their unique material structure and properties. This prompts technological innovations that aid in the the detection and identification of these scientific marvels.

Current detection methods rely heavily on visual identification or with specialised handheld magnetic sensory equipment. This task is labour intensive and requires large amounts of time to survey suspected landing zones. These zones may have hazardous environments that traverse different land formations and as such prove to be unreachable for researchers and enthusiasts. To alleviate these hardships in the discovery of meteorites unmanned aerial vehicles (UAV) may be employed. These versatile vehicles are capable of traversing a multitude of environments with a wide range of temperatures and altitudes. Alongside their affordability and functionality these vehicles are essentially modular thereby making them transformable to suit any sensory needs hence reducing equipment costs and labour.

The design of magnetic sensory equipment can prove to be invaluable and the effects of sensor orientation are throughly investigated in this document. As such, a key component of this project was based on the effectiveness of a pair of fluxgate magnetometers (Stefan Mayer FL1-500) in a dragline setup and their ability to detect the items of interest, meteorites. Through numerous tests based on susceptibility to both relatively strong magnetic fields (as generated

by a bar magnet) and weak magnetic fields (generated from a meteorites residue magnetic field) and the capabilities of the sensors themselves the documents aims to quantify the sensor's usefulness.

In addition to experimental methods, the feasibility of operating the system in conjunction with a micro-controller will provide a plausible system with capabilities ranging from acquisition of sensor data in real time to storage and processing of acquired data to displaying said data either on a display or through wireless communication. However, it is important to note that the preliminary design, prototyping and coding of the sensor suite will have to be refined and completed to allow for actual use in a realistic environment.

Contents

Acknowledgments **iii**

Abstract **vii**

Table of Contents **xi**

List of Figures **xiii**

List of Tables **xvii**

1 Introduction **1**
1.1 Project Scope . . . 3
1.1.1 Goals of the Project . . . 3
1.1.2 Outcome and Deliverables . . . 4

2 Background and Related Work **5**
2.1 Problem Statement . . . 5
2.2 Meteorites found in Australia . . . 5
2.3 Current Meteorite Detection Methods. . . . 6
2.4 Nature of Magnetic Fields . . . 8
2.5 Magnetic Sensors: Introduction to Fluxgate Magnetic Sensors . . . 9
2.5.1 Parallel Fluxgate Magnetic Sensors . . . 10
2.5.2 Orthogonal Fluxgate Magnetic Sensors . . . 11
2.6 Noise . . . 12

3 Project Methodology **15**
3.1 Introduction . . . 15
3.2 Project Considerations . . . 15
3.2.1 Sensor Suite . . . 15
3.2.2 Data . . . 16
3.3 Hardware requirements . . . 16
3.4 Circuit Diagram . . . 22
3.5 Single Sensor Tests . . . 23
3.5.1 Initial Sensor Calibration . . . 23

3.5.2 Directional Response . . . 23
3.5.3 Mapping Magnetic Fields in a Workspace . . . 25
3.5.4 Sensor Susceptibility and Response to External Magnetic Fields . . 26
3.5.5 Sensor Comparison . . . 28
3.6 Dual Sensor Tests . . . 28
3.6.1 Effects of Distance between Sensors . . . 29
3.6.2 Introduction of Magnetic Field to Dual Sensor Setup . . . 29
3.7 Data Collection Methods . . . 29

4 Results and Discussion **31**
4.1 Single Sensor Tests . . . 31
4.1.1 Initial Sensor Calibration . . . 31
4.1.2 Directional Response . . . 32
4.1.3 Mapping Magnetic Fields in a Workspace . . . 35
4.1.4 Sensor Susceptibility and Response to External Magnetic Fields . . 39
4.1.5 Sensor Comparison . . . 43
4.2 Dual Sensor Tests . . . 44
4.2.1 Effects of Distance between Sensors . . . 44
4.2.2 Introduction of Magnetic Field to Dual Sensor Setup . . . 46

5 Conclusions and Future Work **49**

A Oscilloscope Readings **51**
A.1 Results for 4.2.1 . . . 51
A.2 Results for 4.2.2 . . . 52

Bibliography **52**

List of Figures

1.1 *Top down view of: a) Ninety-degree boom orientation. b) Drag-line orientation.* . . . 3

2.1 *Distribution of meteorites as categorised by type, amount and year [4].* . . . 6
2.2 *A geological outlook towards landing zones and meteorites discoveries in Australia [3, 4]. Whilst these maps are accurate they are outdated and as a result it can be surmised that a considerable increase in discoveries in Australia would of occured.* . . . 7
2.3 *Magnetic field properties of a bar magnet [18].* . . . 8
2.4 *Two fundamental parallel fluxgates designs.* . . . 11
2.5 *Basic design structure of an orthogonal fluxgate sensor.* . . . 11
2.6 *Intrinsic noise spectrum graph [32].* . . . 13

3.1 *Basic design specification of: a) the bi-polar supplied FL1-500 sensors [19], alongside pin allocations and dimensions. b) single supply FLC-100 pin allocations and dimension [20].* . . . 16
3.2 *Top down view of the instrumental amplifier alongside pin allocations [6].* . . 18
3.3 *Top down view of the operational amplifier alongside pin allocations [12].* . . 19
3.4 *Pin allocations and form factor of: a) Arduino Uno R3 b)Teensy 3.2. It can be seen that although the headers for the Teensy 3.2 board seem less than for Arduino, the SMH headers on the underside of the micro-controller allows for a total of 34 I/O pins as compared with the 26 I/O pins of the Arduino.* 20
3.5 *Proposed circuit diagram made with Fritzing.* . . . 22
3.6 *Top down view of how the sensors were positioned during the experiments.* 24
3.7 *Top down view of how the workspace was setup.* . . . 25
3.8 *Photograph of the experimental setup on the floor with markings on the the masking tape indicating the measurement positions required of the sensors.* 26
3.9 *Photograph of the sensor setup for the effects that external magnetic material have on the sensor.* . . . 27
3.10 *a)The bar magnet b)Meteorite sample utilised for this experiment.* . . . 28
3.11 *Photograph of the sensor setup for the effects that external magnetic material have on the sensor.* . . . 30

4.1 *Sensor data acquired for position 1 using a DMM following the experimental setup as described in 3.5.2. a) Sensor 1 readings acquired after 3 trails were performed and the associated average, alongside the equivalent magnetic field strength as measured in micro Teslas. b) Sensor 2 readings following the method as sensor 1. When observing readings for position 1 it is revealed that the average output of sensor 1 is greater than sensor 2 by approximately 0.0089V or 0.444μT.* 32
4.2 *Sensor data acquired for position 2 using a DMM following the experimental setup as described in 3.5.2. a) Sensor 1 readings acquired after 3 trails were performed and the associated average, alongside the equivalent magnetic field strength as measured in micro Teslas. b) Sensor 2 readings following the method as sensor 1. When observing readings in position 2 it is revealed that the average output of sensor 1 is greater than sensor 2 by approximately 0.099V or 4.929μT.* 33
4.3 *Sensor data acquired for position 3 using a DMM following the experimental setup as described in 3.5.2. a) Sensor 1 readings acquired after 3 trails were performed and the associated average, alongside the equivalent magnetic field strength as measured in micro Teslas. b) Sensor 2 readings following the method as sensor 1. When observing readings in position 3 it is revealed that the average output of sensor 1 is greater than sensor 2 by approximately 0.266V or 13.279μT.* 34
4.4 *How the theoretical vector value of Earth's Magnetic Field was determined [10].* 35
4.5 *Average magnetic fields (μT) mapped in the allocated 30cm by 30cm workspace as acquired in position 1 a) Sensor 1 readings with incremental readings of 5cm until the limits of the workspace were reached. On average the each move resulted in a magnetic difference of 8.109 μT. b) Sensor 2 readings 1 with incremental readings of 5cm until the limits of the workspace were reached. On average the each move resulted in a magnetic difference of 8.954 μT.* 36
4.6 *Average magnetic fields (μT) mapped in the allocated 30cm by 30cm workspace as acquired in position 2 a) Sensor 1 readings with incremental readings of 5cm until the limits of the workspace were reached. On average the each move resulted in a magnetic difference of 2.442 μT. b) Sensor 2 readings 1 with incremental readings of 5cm until the limits of the workspace were reached. On average the each move resulted in a magnetic difference of 2.740 μT.* 37

4.7 *Average magnetic fields (μT) mapped in the allocated 30cm by 30cm workspace as acquired in position 3 a) Sensor 1 readings with incremental readings of 5cm until the limits of the workspace were reached. On average the each move resulted in a magnetic difference of 5.053 μT. b) Sensor 2 readings 1 with incremental readings of 5cm until the limits of the workspace were reached. On average the each move resulted in a magnetic difference of 5.378 μT.* 38
4.8 *Measured response from the sensor 1 when an external magnetic field is applied. a) Response from a relatively strong magnetic presence, in the form of a bar magnet. b) Response from a relatively weak magnetic material in the form of the meteorite sample. Both samples are separated according to orientation (inline or parallel).* 40
4.9 *Measured response from the sensor 2 when an external magnetic field is applied. a) Response from a relatively strong magnetic presence, in the form of a bar magnet. b) Response from a relatively weak magnetic material in the form of the meteorite sample. Both samples are separated according to orientation (inline or parallel).* 42
4.10 *A noticeable difference can be acquired when utilising the results from the oscilloscope. By converting the voltage output to a magnetic field, the output of the above difference can be calculated and quantified.* 47
4.11 *The dual sensor's response to the meteorite sample is relatively harder to characterise with the oscilloscope readings and hence the resulting graphs do not display an difference that is as clear as with the magnetic response with a bar magnet.* 48

A.1 *The data acquired from P1 indicates the effects on the voltage output of the dual sensor setup as the position is changed by 5cm per reading. Channel 1 represents readings from sensor 1 and channel 2 represents readings from sensor 2.* 51
A.2 *The data acquired from P2 indicates the effects on the voltage output of the dual sensor setup as the position is changed by 5cm per reading. Channel 1 represents readings from sensor 1 and channel 2 represents readings from sensor 2.* 52
A.3 *The data acquired from P3 indicates the effects on the voltage output of the dual sensor setup as the position is changed by 5cm per reading. Channel 1 represents readings from sensor 1 and channel 2 represents readings from sensor 3.* 53
A.4 *Oscilloscope readings as the bar magnet is passed inline with the dual sensor setup.* 54
A.5 *Oscilloscope recording as the bar magnet is passed inline with the dual sensor setup.* 55
A.6 *Oscilloscope recording as the meteorite sample is passed inline with the dual sensor setup.* 56

A.7 *Oscilloscope recording as the meteorite sample is passed inline with the dual sensor setup.* 57

List of Tables

3.1 Specifications comparison between the FL1-500 Fluxgate Magneto-Field Sensors and FLC-100 Single-Axis Magnetic Field Sensors. 17
3.2 Specifications of the INA-125P Instrumental Amplifier 18
3.3 Specifications of the Operational Amplifier: UA741CP or μA741CP 19
3.4 Comparison of micro-controllers Arduino Uno and PRJC's Teensy 3.2 . . . 21

4.1 Directional test summary in terms of average output over 3 trails (3 d.p.). 34
4.2 Workspace Magnetic Gradient as recorded per position 39
4.3 Summarisation on the measurements made in conjunction to both sensor's susceptibility to external magnetic fields. 41
4.4 Summary of outputs for all three positions in a dual sensor setup. 45

Chapter 1

Introduction

Meteorite studies is an area of interest for many scientists ranging from astronomers to enthusiast. The unique characteristics of the meteorite and properties are well sought over; however, current detection and collection methods are labour and resource intensive, requiring large investments, hence, prompting the need for more cost-effective ways for detection.

Unmanned aerial vehicles (UAV) alleviate some of these burdens due to their versatile nature and abilities. These desirable attributes include their ability to traverse a multitude of environments and their ability to produce data at distance, which may aid in the process of detection. However, there still exists a need for an effective sensor array for accurate location identification and meteorites classification. This document proposes a relatively low cost drag-line sensor array, (consisting of two Stefan Mayer FL1- 500 magneto sensors), that will be integrated into a UAV to aid in meteorite detection. This sensor orientation will be thoroughly investigated and their relative advantages and disadvantages discussed. The possibilities of integration in a UAV design architecture is also explored through the use of a micro-controller as a portable microprocessing capture instrument and as a result the sensors suitability for future applications in a prototype.

There has been some prior research into boom configuration sensors [24] for meteorite detection, however it was concluded that a trade-off between sensitivity and existed (the sensor array would be required to fly close to the ground to acquire accurate data). Also the speed at which a drone passes over a stationary meteorite seemed to have affected the resolution of the acquired readings. This effectively meant that the UAV would need to be within approximately 0.05 meters of the ground and flying at around 2 - 3 meters per second to have conclusive sensor readings. As the distance from the ground increased it was found that the output signal would become inconclusive and hard to differentiate with environmental noise present. Similarly, the same was found with the velocity at which the drone travelled, the sampling speed of the sensors used could not keep up with the rate at which the meteorite was passed under the array. These results prompted the need for research into alternative designs that will not be limited by these restriction and an approach to alleviate the opportunity for inaccurate readings.

The proposed dragline sensor orientation would allow for an increase in geographic

coverage and reduction in human resources. However this sensor orientation does come with its own shortcomings which includes the increased risk of damage to the sensor suite/array due to environmental obstacles and desynchronisation of the sensors themselves. This being stated the proposed dragline system will utilise different sensors (Stefan Mayer FL1-500) as compared to the experimental boom configuration (Stefan Mayer FLC-100) and as such require thorough sensor testing to characterise the performance in detection of magnetic fields alongside the resolution of collected data.

This being stated, the use of the completed sensor suite will not be limited to meteorite detection but as a research platform for future autonomous sensor suites that can implemented in a variety of different environments. This includes applications such as: agricultural or geological surveying or in war relief efforts as an unexploded ordinance locator and hobby uses such as a autonomous metal detection.

1.1 Project Scope

1.1.1 Goals of the Project

- **Short term goal**: Provide a comprehensive sensor analysis for the FL1-500 fluxgate magnetic field sensor and determine its usefulness in a drag-line configuration.
- **Long term goal**: Prototype the sensor suite with the use of an Arduino Uno or any other relatively small micro-controller as a means of data capture and storage. Also, to integrate the sensor suite/array into an existing UAV for operational testing.

The main requirement of this project is to provide a useful and in depth insight into the operational prowess of the Stefan Mayer FL1-500 fluxgate magnetic field sensors for use in a drag-line configuration. To establish this, a sensor test-bed was established to determine the confines of the sensors and a decision based on the findings will indicate if these sensors are feasible and suited for its intended operation or if the single axis FLC-100 sensors are favourable.This in turn can be considered the short-term goals.

The long-term goal of this project is the design and prototyping of a drag line sensor alongside operational coding to allow for applications in meteorite surveying. This sensor will have to be designed and tested in different environments and conditions to allow for application in varying conditions. In turn this will provide a defined conclusion whether a dragline sensor or a boom sensor will be favourable in the use of meteorite detection. The aforementioned sensor orientations are displayed below in Figure 1.1.

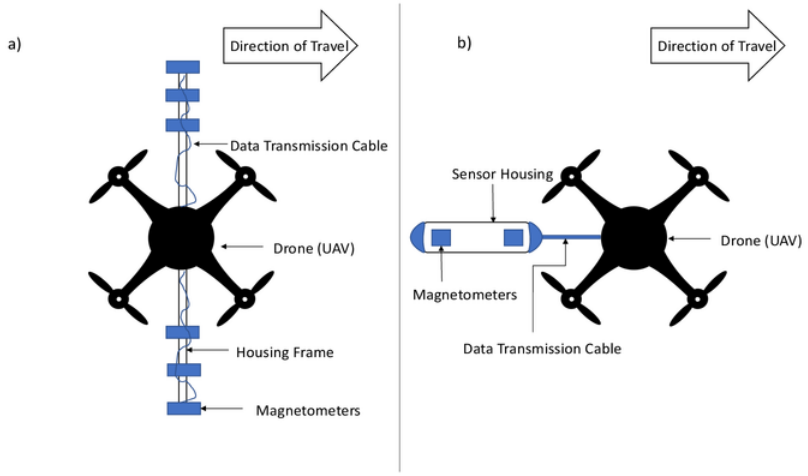

Figure 1.1: *Top down view of: a) Ninety-degree boom orientation. b) Drag-line orientation.*

1.1.2 Outcome and Deliverables

The expected outcome of this project is as follows:

- A documented performance report on the FL1-500 sensors and their corresponding application in a drag-line orientated sensor array.

This outcome is expected to be completed in the allocated time frame and can be considered the deliverables of the project. These deliverables would also include an experimental procedure stating the acquisition method for operational data and simulation data based on the performance of both sensory arrays. If further development based on the outcome can be achieved, a prototype of the drag-line sensor can be created and integrated into a relevant UAV's design architecture.

Chapter 2

Background and Related Work

2.1 Problem Statement

The undermining research topic incorporates an investigation into how magnetic fields function, and circuit elements that can successfully identify weak magnetic fields produced by meteorites. Recent developments or technologies employed in the field of meteorite detection are also investigated.

2.2 Meteorites found in Australia

Historically, Australia does not have as high of a fall to find ratio (1 in every 20) [4] when compared to countries such as America (1 in every 7), however, this has been accounted as a result of a rather non-uniform-ally distributed and sparse population. There exists a host of other factors as to why this is the case with some environmental (dense vegetation, wet climate; congruent with tropical Australia) and some due to lack of education or recognition [4]. This being stated, this does not undermine the fact that there have been multiple discoveries ranging from the first documented case in 1854 near Cranbourne [5], Victoria to 1992 as shown in Figure 2.1. A geological map of landings and meteorite discoveries further solidifies this fact and as shown in Figure 2.2 Western Australia has relatively more discoveries. As of 1992, it was officially documented that a total of 277 distinct meteorites were discovered with varying numbers across all categories of meteorites and within the span of four years the number had increased to 477 meteorites. The categories incorporated can be found in the following table.

The Nullarbor region in Western and South Australia, in particular, is considered one of the most meteorite rich desert environments, second only to Antartica and accounts for roughly fifty percent of Australia's meteorite discoveries [3]. Due to the high limestone content of the surrounding area and the direct contrast with meteorites' brownish exterior alongside the lack of heavy foliage or vegetation due to the arid environment surrounding this region, the meteorites become visually identifiable and therefore easily retrieved and documented. When compared to the subtropical and more urban areas, the more arid,

locations are more favourable and as a result areas of stated environments tend to have less discoveries such as Queensland or New South Wales. This being stated more destitute areas such as the deserts in central Australia also yield less discoveries due to the nature of surrounding areas. Sand becomes an obstacle for not only traversing the landscape but also for covering any visual semblance of meteorites, hence prompting the need for versatile equipment capable of detecting faint magnetic fields whilst also being able to discern the meteorite from other potentially ferromagnetic materials.

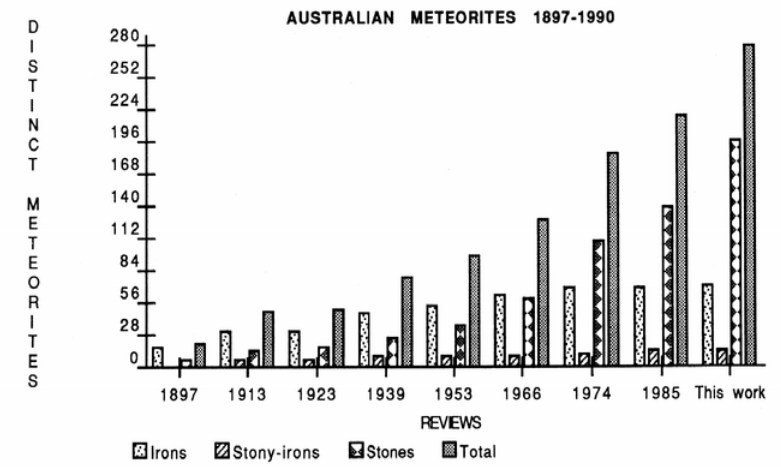

Figure 2.1: *Distribution of meteorites as categorised by type, amount and year [4].*

2.3 Current Meteorite Detection Methods.

The strength of a meteorite's magnetic field depend heavily on it's iron-nickel (Fe-Ni) composition and hence why sensors that can sense relatively weak magnetic fields were sought after to locate them. Prior to the use of magnetic sensors, detection methods required the use of visual or handheld electromagnetic devices [9] and were considered labour intensive, requiring physical land surveying in possible meteorite landing zones . The aforementioned detection method has declined in viability due to an increase in surrounding terrestrial rock formations that interfere with data collection by electromagnetic devices, hence prompting the need for design alternatives to compensate for possible labour cost increases [9]. One design alternative incorporated the use of magnetic sensors.

Magnetic sensors were commonly employed to locate/resonate with the degrading magnetic fields produced by iron, stony iron and chondrite meteorites [25]. However, there are many samples located on Earth that have little to no ferromagnetic material such as achondrites. These types of meteorites are ultimately indistinguishable when compared to other rock formations, especially when considering their susceptibility to

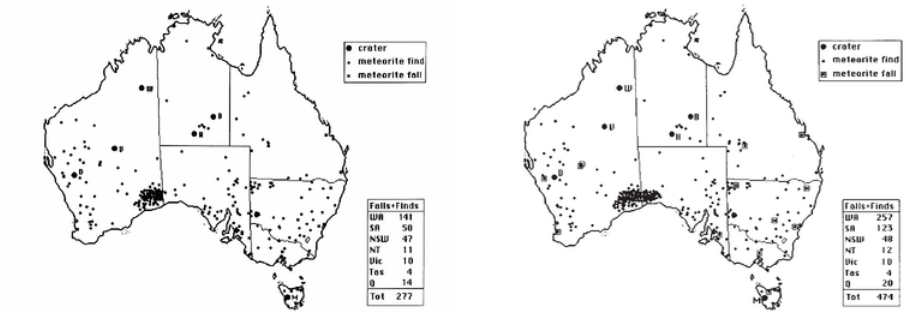

(a) *Discoveries made in 1992* **(b)** *Discoveries made in 1996*

Figure 2.2: *A geological outlook towards landing zones and meteorites discoveries in Australia [3, 4]. Whilst these maps are accurate they are outdated and as a result it can be surmised that a considerable increase in discoveries in Australia would of occured.*

magnetic field sensing elements. High powered radars, alongside multi-spectral imaging techniques, were methods used regularly to circumvent this problem in meteor prone locations such as Antartica [1, 33]. This being stated, the equipment cost was relatively high proving the method was effective but not very cost effective in large areas [33].

In recent times, there has been an increase in interest for research into autonomous meteorite detection methods utilising machine learning technology and various spectral imaging technologies [8, 22, 31]. Essentially this area of research has made viable, a mode of transportation (usually airborne) that can function without an authorising personnel whilst also automatically identifying and pinning the location of possible meteorite pieces by employing nothing more than a camera module and convolutional neural networks capable of comparing collected data with a pre-updated digital library consisting of images obtained from the internet [31]. By labelling the sample images with positive or negative matches, the image classifier would be able to discern different physical characteristics that adhere to classical meteorite structures. Augmentations to the positive images were made (orientation, contrast, reflection, resolution, brightness and saturation) and as a result accuracy is further increased [8]. This method produced rather consistent results in plain environments (two out of two meteorite detected with minimal false positives) but in inclines or rocky environments the accuracy decreased (two out of two meteorite detected with many false positives.) [8, 31].

Due to this field being relatively new and the nature of technology (always evolving), though, improvements in classification schemes, decrease in image processing times and methods for test image collection are under consideration to allow for more accurate identification/profiling means [8].

This being stated, the main goal of this project is the comparison of data based on magnetic field readings. Therefore, attention will be emphasised on understanding magnetic fields and how magnetic sensors utilised in the project function in order to

locate meteorites in terrestrial environments.

2.4 Nature of Magnetic Fields

Magnetic fields and how they are detected are underlying theories relating to this project and a fundamental understanding is required to fully acknowledge the methods utilised. Magnetic fields, $\vec{H}$, are vector measurements containing both magnitude and direction and can be easily described by observing the functionality of a bar magnet, as shown below.

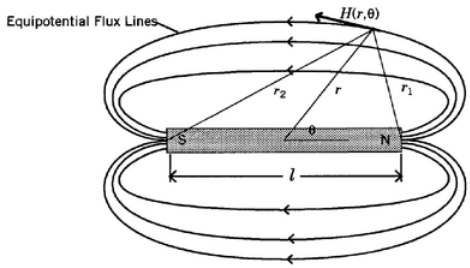

Figure 2.3: *Magnetic field properties of a bar magnet [18].*

The following mathematical expression can be derived to show the relationship of magnetic field, $\vec{H}$, when measured at a distance much greater than the longest dimension of the bar magnet [18]:

$$\vec{H} = \frac{3(\vec{m} \times \hat{a_r})\hat{a_r} - \vec{m}}{r^3} \tag{2.1}$$

Where r is the distance between magnetic source and measurement point, $\hat{a_r}$ is the unit vector along r and m is the magnetic dipole moment. Other important vectors that share a relationship with magnetic fields includes: strength and intensity (known as magnetisation $\vec{M}$, with units moments per unit volume) and flux density or magnetic induction ($\vec{B}$ with units density of magnetic flux per unit area). It is important to note that magnetic flux represents the strength or flow of magnetic field in an area, whilst magnetic field strength is a measure of force. The corresponding relationships are shown in the equations below:

$$\vec{B} = \mu_0 \vec{H} \tag{2.2}$$

$$\vec{B} = \mu_0 (\vec{H} + \vec{M}) \tag{2.3}$$

$$\vec{M} = \chi \vec{H} \tag{2.4}$$

Where μ_0 is the magnetic permeability in free space and χ is a vector quantity in isotropic materials representing the magnetic susceptibility of a material. Now relating this to meteorites, it is important to know that the magnetic field strength and susceptibility are based around the ferromagnetic content (Fe-Ni metal, schreibersite, cohenite, magnetite, and pyrrhotite [29]) found within the meteorite's structure. This content directly relates to the classification of meteorites and their susceptibility to magnetic fields with chondrites groups usually having a larger mean metal content and achondrites groups usually having less [28–30]. However, it is important to note that magnetic susceptibility lowers with deformity, terrestrial weathering (oxidation of metal content) and anisotropic meteorites. This rate was described as logarithmic and varies according to location and base physical structure of the meteorite in question [29]. Most meteorites are however, anisotropic hence making it hard to quantity the magnetic susceptibility, unless specific instruments such as the SM30 shirt pocket-sized magnetic susceptibility meter [13] (manufactured by ZH Instruments) is used to acquire an average in all vector directions.

2.5 Magnetic Sensors: Introduction to Fluxgate Magnetic Sensors

There are many commercially available magnetic sensors, however due to the fact that a fluxgate sensor is being applied, this section will focus on fluxgate magnetic sensors. Fluxgate sensors are one of the most widely utilised magnetic sensors that can measure both the intensity and orientation of magnetic flux lines [17]. This type of sensor has the following advantages over other types of magnetic sensors:

- Physically small and durable.
- Very energy efficient, require low input voltages.
- Large sensitivity range.
- Low noise disturbances and high stability outputs.
- Large operating bandwidth.

These sensors function through the use of a fluxgate, a transducer that essentially converts magnetic field into electrical voltage [18]. This type of sensor utilises this type of technology and follows Faradays laws, stating that any loop of wire that is subjected to a changing magnetic flux induces a voltage within the loop, proportional to the rate of change of flux [18]. As a ferrous material (in this case, a meteorite) approaches the signal sensing axis/coil, it induces a change in saturation (from low to high) of magnetic flux within the core and as a result a voltage will develop at the terminal proportional to this change, hence producing an analog voltage reading. The following equations establish this relationship:

$$e(t) = nA\frac{d(\mu_e\mu_0 H)}{dt} \tag{2.5}$$

Where: n is the number of wire turns on the signal windings, A the cross-sectional area, μ_e the permeability of the core, μ_0 the magnetic permeability of the material measured and H the magnetic field being measured [18]. It is important to note that all these factors are measured with respect to time.

There exists two natural orientations that fluxgate sensors can be created/manufactured in: orthogonal and parallel, however the fundamental principles underlying both sensors of remain the same with the main difference being the way the sensory coil is positioned.

2.5.1 Parallel Fluxgate Magnetic Sensors

The principles and fundamentals of parallel fluxgate magnetic sensors date back to the 1930s [11] whilst innovations in the different fields such as sensor noise mitigation and core material selection has helped further refine these principles and therefore increased the functionality and possible applications of said sensors [27]. The basic form of said sensor can be seen in Figure 2.4a. It is important to note that all the necessary components that encompass this model; the time-varying excitation flux Φ_E, the excitation field intensity H_E and measured field H_M, are all in parallel with each other. All the above variables are dependant on each other with the excitation flux, being generated in the ferromagnetic core, in direct correspondence with the excitation field strength and the field strength produced by the excitation coil. Basically speaking the magnetic core is periodically saturated in both directions by the magnetic field generated by the excitation field and the measured field. As an external field is applied in an axial direction an even harmonic output voltage can be observed [7], [23] due to the asymmetry produced in the measurement windings. However, if the no external magnetic field is present the electromotive force (EMF) induced in the measuring winding would output an odd harmonic due to the excitation current. This odd harmonic is usually cancelled out by the sensor's natural configuration such that the mutual inductance between both excitation and measurement windings are kept to a minimal. It can be noted that the core can be of race tack or ring core configured. Typically the voltage output at the terminals can be contributed due to induction law and can be calculated with the following equation [14]:

$$U_i = -N \times S \times (\frac{dB_E}{dt} + K \times \mu_0\mu_r \times \frac{dH_M}{dt} + K \times \mu_0 \times H_M\frac{d\mu_r}{dt}) \tag{2.6}$$

where H_M is the external magnetic field intensity (which will become time-varying as the sensor is used), B_E is the alternating excitation flux density found in the ferromagnetic core of the sensor caused by the excitation field intensity H_E, N is the number of turns of the coil (used to pick-up variations in field strength), S the core's cross-sectional area, μ_0 the permeability of a vacuum and K is a coupling coefficient of the core to the field H_M which is effectively dimensionless.

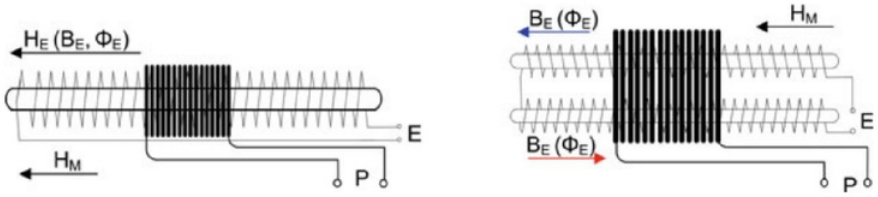

(a) *Simple single core parallel fluxgate design [14]* **(b)** *A two core variation on the simple design [14]*

Figure 2.4: *Two fundamental parallel fluxgates designs.*

It must be noted that a blatant disadvantage of this type of orientation exists and that can be seen in the first term within the parenthesis. The simple sensor essentially incorporates the excitation flux into the pickup coil which will provide false readings when high sensitivity readings are required. This being stated the most important term undermining the principles of fluxgates can be found in the last term within the parenthesis. This term represents the alternating excitation field H_E which periodically switches the saturation levels of the magnetic materials utilised in the fluxgate core [14] which modulates the permeability of the core itself.

Parallel fluxgates however are very versatile sensors being utilised in all different applications ranging from magnetometers to unexploded explosive ordinance tracking and gradiometers [18]. It is important to note that this type of sensor will be utilised in its simplest form as the magnetometer of choice in this project.

2.5.2 Orthogonal Fluxgate Magnetic Sensors

Orthogonal fluxgates follow similar principles as parallel fluxgate sensors however they differ in their structure as shown below in Figure 2.5.

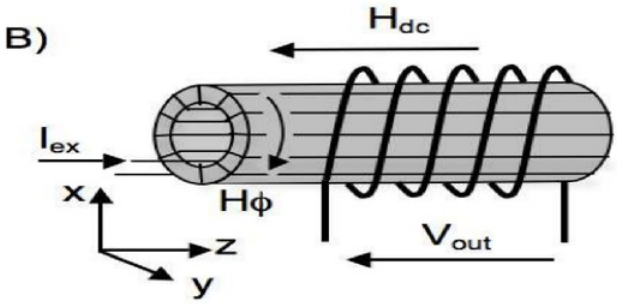

Figure 2.5: *Basic design structure of an orthogonal fluxgate sensor.*

The core of the sensor is usually comprised of a soft magnetic material in the form of a cylinder, with an excitation coil wrapped around it. The direction that the excitation current flows through the coil is important in this case as it represents the direction that excitation occurs H_ϕ around the circumference. When operating, the core is periodically saturated in opposite polarities as caused by H_ϕ and the voltage output detected by the pick-up coil. The external field H_{dc} in this case is the same as the field in parallel fluxgates meaning that $H_{dc} = H_M$ and is applied in the axial direction. The origin of the name comes from the fact that the measured field or H_{dc} is orthogonal to the x-y plane where the excitation field can be located [7].

The magnetic sensors utilising these principles are usually well sought after due to the minimalistic design when considering the fact that micro-wires can be used to simulate the fluxgate core. This type of core-less design allows for the excitation current I_{EX} to flow through the wires causing a circumferential field being developed H_ϕ while the pick-up coil is still wound on the outside [7]. By following this method of design, the manufacturing cost and complexities decreased allowing for current applications where highly miniaturised sensors were required [11]. Similarily the following advantages and disadvantages are given when comparing orthogonal to parallel fluxgate sensors:

Advantages:

- They have high spatial resolution which is only limited by the wire diameter used for the core.
- Smaller structure due to lack of excitation coil.
- Ease of manufacturing .
- Low excitation current (tens of mAs compared to parallel fluxgate cores with a few hundred mAs)

Disadvantages:

- Experience more noise than parallel fluxgates.
- Lower sensitivity due to small wire cross-sectional areas
- The excitation current that flows through wire core can undergo power dissipation, increasing the temperature of the wires and therefore becoming a source fro noise.

2.6 Noise

Noise is a undesirable characteristic present in all analogue/digital sensors or modules. This is due to the fact that it causes distortions/ fluctuation in acquired data causing devices needing high order of accuracy to not function as needed.This is especially detrimental to measurement units such as magneto sensors due to the high level of accuracy required to discern ferromagnetic material from meteorites.There are two distinct categories of noise, extrinsic (interference) and intrinsic (inherent) [21].These types of noise

can be periodic, intermittent, or random. Electrical, magnetic and motor noise are forms of extrinsic noise. Intrinsic noise are described as random processes due to the fact that they vary with quantum fluctuation which is present in all resistive and semi- conductive materials that can create/reduce current and voltage inside a circuit [21]. It is important to note that there is no way to remove noise but only ways to minimise its effects. Some examples and sources of noise include:

1. **White Noise, Pink Noise, And Noise Floor:** The noise floor is the lowest or base level of intrinsic noise. White noise is known as broadband noise and is the voltage noise present in all intrinsic measurements. Pink noise (also known as flicker or 1/f noise) only occurs when current flows and is captured and released randomly causing fluctuations in current [32]. These types of noise are represented in intrinsic noise spectrum as seen in Figure 3.1

2. **Schottky Noise (Shot):** This type of noise occurs as a subset of white noise. It occurs whenever current passes a PN junction inside of semiconductors and excited electrons leave electron-hole pairs [32].

3. **Johnson Noise (Thermal):** This type of noise occurs whenever thermal energy or heat agitates electrons within resistors or other elements with gain such as instrumental amplifiers and operational amplifiers [32].

4. **Resistor Noise:** This type of noise occurs in all resistors and is caused by movement of charge and thermal energy [32].

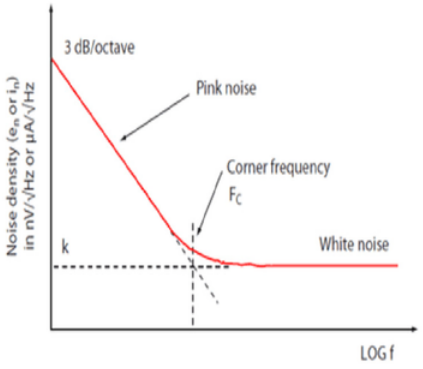

Figure 2.6: *Intrinsic noise spectrum graph [32].*

The most prominent source of noise for measurements utilising magneto sensors is Johnson noise. This noise is considered the voltage associated with the motion that electrons would travel when temperatures above absolute zero or when thermal energy is

available. Due to the fact that even all voltage sources have some resistance all voltages will eventually develop Johnson noise. Johnson noise or thermal noise is also responsible for the somewhat infamous units of root hertz noise or $\sqrt{Hz}$. These units arise when observing the mathematical model for this type of noise. Noise voltage can be calculated by the following equation [15]:

$$V = \sqrt{4kTBR} \tag{2.7}$$

Where, V is the rms noise voltage developed in any resistance source, k is the Boltzmann's constant of $1.38 \times 10^{-23} joules/K$, T the absolute temperature in Kelvin, B, the bandwidth of noise in Hz and R the source's resistance in Ohms [15]. The thermal noise is white in nature as it contains constant noise power density per unit bandwidth. It must be stated that root hertz noise is usually used to describe the spectral density of noise as a root mean square value over a given bandwidth. To mitigate this type of noise the temperature of all electronic components in both the sensor suite and UAV will have to be minimised either by providing sufficient heat sinks or decreasing the number of components in the system. Another way to reduce noise is to decrease the bandwidth to increase the response time however this method is not really desirable in this application due to the fact that the sensor suite will have to provide real time readings for analysis.

Chapter 3

Project Methodology

3.1 Introduction

This chapter will detail the experimental procedure required to provide a thorough sensor operational. It will also incorporate a list of hardware required to complete the experiment alongside a proposed circuit diagram required to initialise and utilise the magneto-sensors.

3.2 Project Considerations

The following subsections aims to discuss the initial considerations required to form the basic concepts and tests that a design will have to complete to progress towards prototyping . These key components and concepts encompass the materials and equipment which this project is predicated on as well.

3.2.1 Sensor Suite

The main objective of the sensor suite is to be versatile and robust whilst also remaining accurate and of a small form factor alongside being relatively noise free when detecting any trace of residue magnetic fields produced by meteorites. The functionality and performance of the sensors will first be addressed in a laboratory environment so that all possible conditions can be tested. The responsiveness of the sensors within this environment will provide an experimental base to compare theory with results acquired throughout use in the suite intended environment. This being stated one of the most important considerations when considering the suite's design is its form factor due to the limited spacial and weight limitations placed on a portable sensor array when considering applications in UAV design architecture. Also, power management can be integral depending on duration of use and surveying distance and in saying so the sensor suite must perform as intended whilst also being energy efficient.

3.2.2 Data

The collected data will need to be processed, stored and formatted in such a way that any demographic user can easily identify the location and type of meteorite indicated by the data. The data will need to be also relatively small in size as well to facilitate longer use before memory is filled but also ensure ease of integration into user selected applications and interfaces so that post data analysis can be available. Also the data from the physical tests must be identified for the sole purpose of sensor or device calibration to ensure that results from any test is valid and acknowledgeable.

3.3 Hardware requirements

Magnetometer: FL1-500
The FL1-500 Single Axis Fluxgate Magnetometer from Stefan Mayer Instruments is a high precision magnetometer with relatively high sensitivity. Designed to measure fields of up to $\pm 500 \mu T$, this sensor has a wider measurement range when compared with standard single axis sensors such as the FLC-100 but as a downside, requires more power to function. This being stated, when considering usage in a UAV environment it may be advised that a voltage booster in the form of chopper drivers or anything of similar effect be required alongside these sensors to aid or pull up to voltage to suit the sensors needs. Also the FL1-500 sensors have less noise which could help acquire more accurate results.The main reason this sensor is utilised is the effective measurement range and its effectiveness in locating weakened magnetic fields, hence making them a perfect meteorite hunting tool.

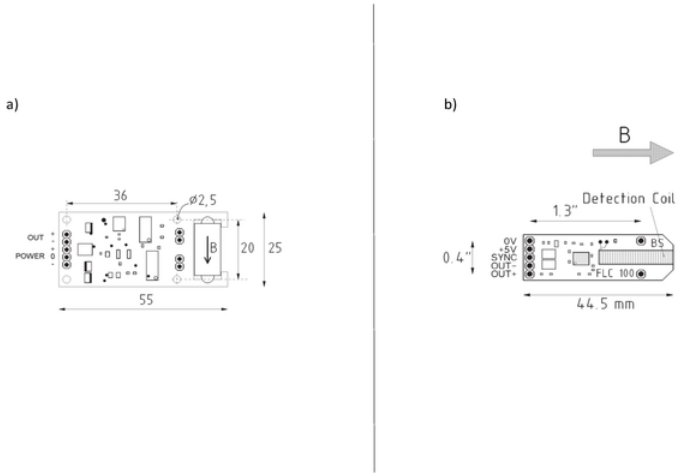

Figure 3.1: *Basic design specification of: a) the bi-polar supplied FL1-500 sensors [19], alongside pin allocations and dimensions. b) single supply FLC-100 pin allocations and dimension [20].*

Table 3.1: Specifications comparison between the FL1-500 Fluxgate Magneto-Field Sensors and FLC-100 Single-Axis Magnetic Field Sensors.

	FL1-500	FLC-100
Supply Voltage (V)	±12 to 16	5V single supply
Operating Temperature (°C)	0 to +70	-40 to +85
Analogue Output Voltage (V)	0.02 / μT, max. ±10	± 1 / 50 μT, max.±2.5
Bandwidth (kHz)	0 to 1 (-3dB)	0 to 1 (-3dB)
Noise ($pT/\sqrt{Hz}$)	less than 20 at 1 Hz	≈ 150 at 1 Hz
Calibration Accuracy	0.5 %	0.2 %
Measurement Range (μT)	± 500	± 100

For more information, please see the respective data sheet [19].

Prior research has been completed utilising the Stefan Mayer's FLC-100 sensors. These sensors have different operational specifications when compared with Stefan Mayer's FL1-500 resulting in the need to investigate the capabilities of the new sensors. It is important to acknowledge that both types of sensors were supplied by the Department of Earth and Planetary Sciences. However, due to the fact that the FLC-100 sensors were in use by another student, the only sensors available were the FL1-500 sensors.

Instrumental Amplifier: INA125-P

INA-125P is a low- power, high accuracy instrumental amplifier with precision voltage reference. It also has adjustable gain which can be achieved by adding a resistor corresponding to this formula:

$$Gain = 4 + \frac{60k\Omega}{R_G} \tag{3.1}$$

Where R_G= variable resistor chosen corresponding to gain. It is important to note that gain identification or selection is a major consideration due to it being proportional to the output sensitivity of the sensors and as as result noise as well. Therefore to choose an appropriate gain, both instrumental amplifier and sensor's noise levels would have to be minimised and the desired analogue output of the sensors would have be within the amplifier's measurement sensitivity range. Another important tool available is the voltage reference which provides an accurate and stable output source for sensor applications. As a rule of thumb though, the desired positive supply voltage must be 1.25V above the desired reference [6].

$$V_O = ({V_{IN}}^+ - {V_{IN}}^-)G \tag{3.2}$$

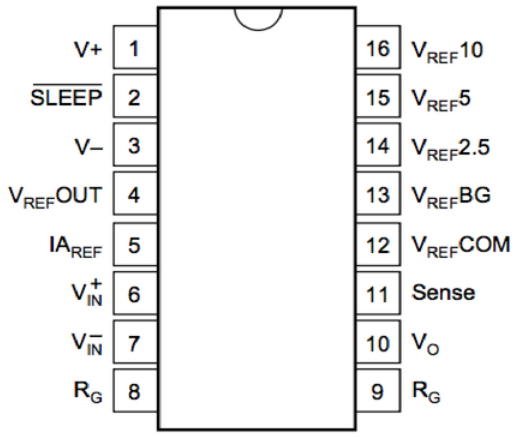

Figure 3.2: *Top down view of the instrumental amplifier alongside pin allocations [6].*

Table 3.2: Specifications of the INA-125P Instrumental Amplifier

INA-125P Instrumental Amplifier [6]	
Supply Voltage (V)	−40 to +40
Quiescent Current (μA)	460, max. 525
Operating Temperature (°C)	-55 to +125
Output Voltage (V)	Positive: 1.2, Negative: 0.3
Bandwidth (kHz)	0 to 1
Noise (nV/ $\sqrt{Hz}$)	38 at 1kHz

In the overarching circuit design the INA125P instrumental amplifier plays a large role in amplifying the differences between the two fluxgate sensors. Essentially, this amplifier acts as a differential comparator allowing for two input signals to be compared and the difference between the input voltages multiplied by a gain set by the formula stated above (Equation 3.2). Since the acquired differences can be minuscule in comparison to overall sensor outputs, the amplifier helps administrating a gain large enough to make this difference noticeable by both user and micro-controller, therefore making this module one of the most crucial in terms of electrical circuit design.

Operational Amplifier: UA741CP or μA741CP

UA741CP or μA741CP is part of a family of general purpose operational amplifiers capable of allowing offset-voltage nulling [12]. In the electrical design of the magnetic sensory system, this operational amplifier was utilised in a closed loop as a inverting voltage gain amplifier following classic op-amp theory and calculations:

Table 3.3: Specifications of the Operational Amplifier: UA741CP or μA741CP

Operational Amplifier: UA741CP or μA741CP [12]	
Supply Voltage (V)	-15 to $+15$
Supply Current (mA)	2.8 at 25°C, max. 3.3
Input Offset Current (nA)	200 at 25°C, max. 300
Operating Temperature (°C)	0 to +70
Total Power Dissipation (mW)	85 at 25°C, max. 100

$$Gain = \frac{V_{out}}{V_{in}} = -\frac{R_f}{R_{in}} \tag{3.3}$$

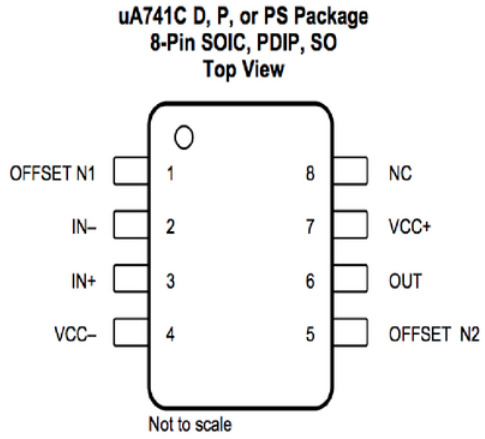

Figure 3.3: *Top down view of the operational amplifier alongside pin allocations [12].*

Where R_f = feedback resistor and R_{in} = input resistor. The primary reason that this operational amplifier must be utilised is mainly due to the sensor's use in conjunction with the micro-controller. When the fluxgate sensors output a negative voltage reading the micro-controller will not be able to acquire this signal due to the fact that the analog input range of the micro-controller used in general testing was strictly limited to +0 to $+5V$. However, when the sensors are used in conjunction with the UA741CP or μA741CP, the sensor output will become inverted to a positive reading therefore allowing for the micro-controller to acquire said readings. The operational amplifier was not be used with any gain as there was no need for the output signal to become any greater. It must be

noted that each sensor must be connected to a operational amplifier as both could output a negative voltage and hence require inversion. This will be further displayed in the circuit diagram in section 3.4.

Microcontroller (Arduino Uno/ Teensy 3.2)
The micro-controller is a integral component of the overarching sensor suite design due to its capabilities of not only storing data but also as a way to process and acquire the differences between the sensor outputs. The Arduino Uno [2] was the initial coding tool due to its functionality and portablity as a usb-based micro-controller compatible with its own encoding software and language (Arduino IDE). Although the design profile/form factor of the Uno board is larger than the Teensy 3.2 micro-controller from PRJC [26] it is still a useful tool in the identification and initial testing of the sensor's connectivity with the allocated micro-controllers. The form factors and input/output (I/O) pins of both micro-controllers are shown below in Figure 3.4.

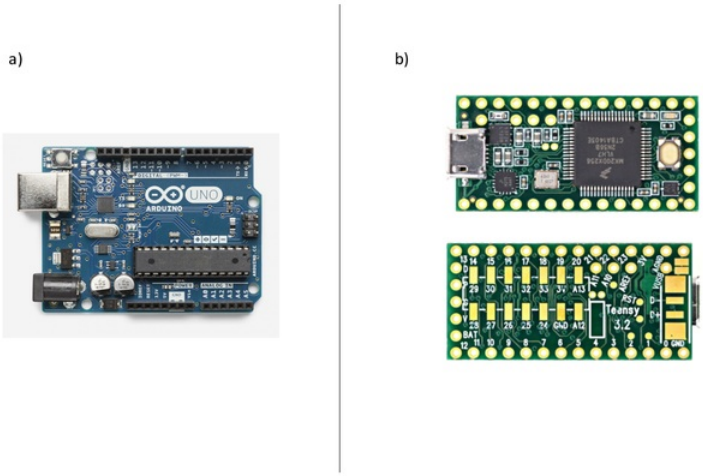

Figure 3.4: *Pin allocations and form factor of: a) Arduino Uno R3 b)Teensy 3.2. It can be seen that although the headers for the Teensy 3.2 board seem less than for Arduino, the SMH headers on the underside of the micro-controller allows for a total of 34 I/O pins as compared with the 26 I/O pins of the Arduino.*

Further development of the sensor suite would favour the Teensy 3.2 due to the numerous I/O pins available and the form factor. Both micro-controllers are usb powered and suit the needs of the sensor suite however due to the onboard capabilities of the Teensy 3.2 (as a self contained board) with which can emulate multiple components such as digital to analog converters (DACs), the Teensy 3.2 is more favourable due to the minimisation

Table 3.4: Comparison of micro-controllers Arduino Uno and PRJC's Teensy 3.2

	Arduino Uno	**PRJC's Teensy 3.2**
Supply Voltage (V)	6 to 20	5
Analog I/O Pins	6	21
Digital I/O Pins	14	34
Dimensions (mm)	68.6 × 53.4	35.56 × 17.78
Price ($USD)	$22	$19.80

of external circuitry. Also the limited analog I/O pins of the Arduino board would prove limiting if more sensors or inputs are required. Therefore if the sensor suite is deployed as a drone platform sensor, the Teensy 3.2 is recommended. The main characteristics of this sensor are highlighted below:

- Extensive software support (Windows, Macintosh OSX and Linux) [26] within the Arduino IDE design environment.
- Comes with assorted I/O pin allocations (audio, analogue, digital and power).
- Can emulate multiple components such as converters, comparators and DACs, hence saving component space in a UAV design environment.
- Relatively cost effective.

3.4 Circuit Diagram

Figure 3.5 represents the proposed circuit diagram incorporating the bare minimal electrical components required for this project. It can be noted that a LCD screen or display can be added to this design as a way of displaying the data received from the sensors. Due to the fact that the sample hobby UAV received from the Department of Engineering, had a LCD display to track power management and synchronisation of the motors on the UAV, it is within the design philosophy to include the sensor suite and by interfacing with a display, provide a visual reading from the suite.

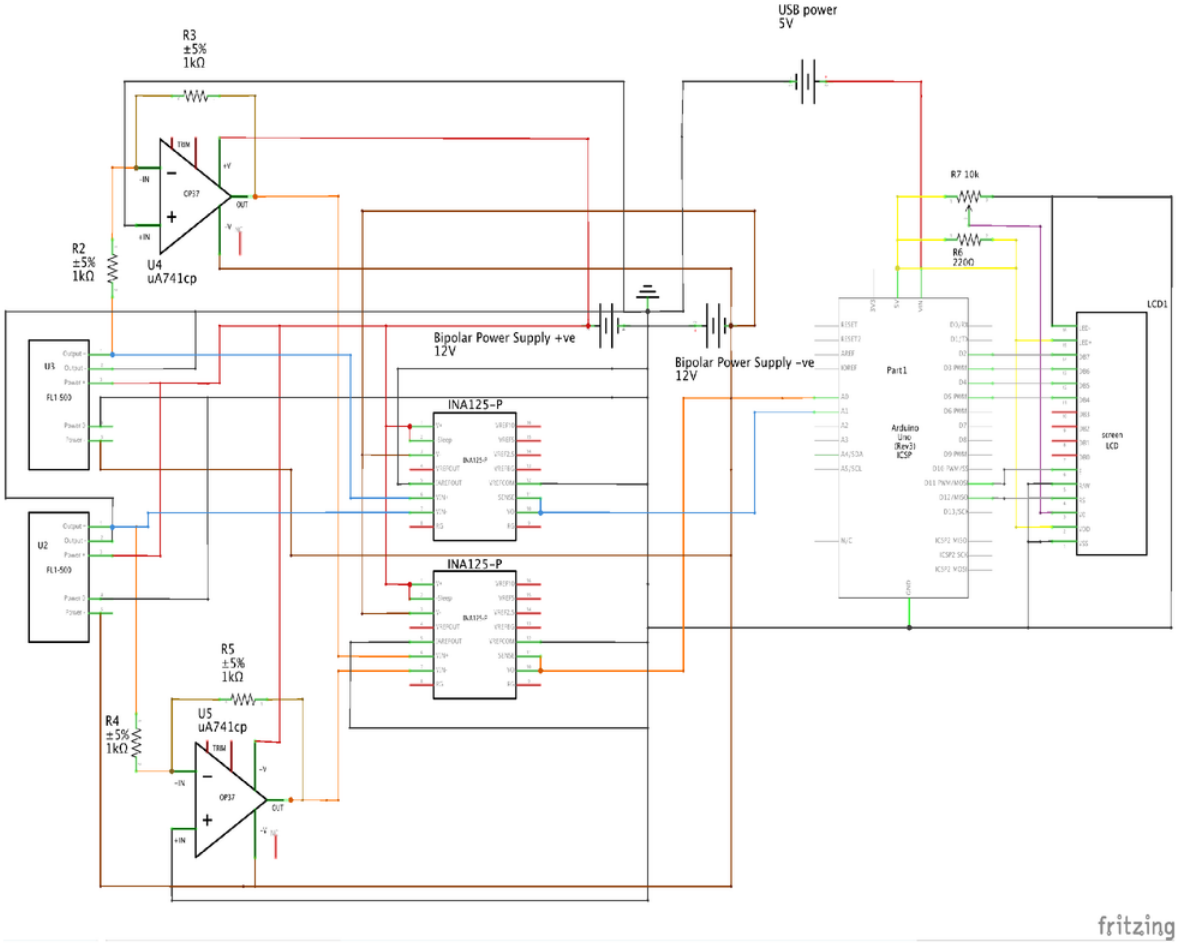

Figure 3.5: *Proposed circuit diagram made with Fritzing.*

The logic behind the circuit diagram is as follows; since the Arduino Uno R3 board has a limited analog input range (0V-5V) and the sensors can produce a positive or negative signal, two inverting operational amplifiers (UA741CP or μA741CP), one per sensor, can be used to invert the negative output to a positive signal. Following this the now positive signal will be passed though an instrumental amplifier (INA125-P) to have the difference compared and gain amplified by a predetermined gain (depending on how small the difference is). Depending on the saturation of the sensor's coils, a positive output will not be inverted but will have to be passed, untouched, to the instrumental amplifiers (INA125-P) where a similar set of operations take place and passed the final results communicated to the Arduino for post measurement processing, storage or display.

3.5 Single Sensor Tests

This section will involve the experimental tests completed on each of the two sensors to identify individual performance characteristics. These tests were completed before observing how the dual sensor setup will perform and ideally allow an investigation as to whether the sensors affect each others readings if used in tandem with each other. It must be noted that the sampling speed of the sensors are an integral characteristic that needs to be explored, however due to time constraints could not be accomplished.

3.5.1 Initial Sensor Calibration

It is imperative to acknowledge the fact that two dual sensor setup must be used in tandem to correctly account for the presence of meteoric material as compared to a single sensor setup. This is mainly due to the fact that a dual sensor setup allows for a difference between the two sensors to exist, with the difference representing the main detection method. For example, when a single sensor passes over a unknown ferromagnetic material deposit it would alert the user that a magnetic presence is located and hence provide false information that a meteorite is located. However, if a dual sensor suite is deployed and passes through the hypothetical metal deposit, the difference between the sensor output would essentially become zero as both sensors sense the same material and produce a similar voltage/magnetic field response. This being stated if a meteorite is present as the sensor suite enters the meteorites magnetic field, the first sensor's outputted voltage may be large, however, since the difference between the two sensors is the detection method, the reading will be recorded and only when a noticeable difference in the entire profile can be seen will a meteorite be identified.Therefore before the sensors can be used in tandem with each other, the individual zero drift characteristics of both sensors must be explored.

3.5.2 Directional Response

This is essential to insure that both sensors will provide an accurate response prior to being gain amplified by the instrumental amplifier. To accomplish this, each sensor must

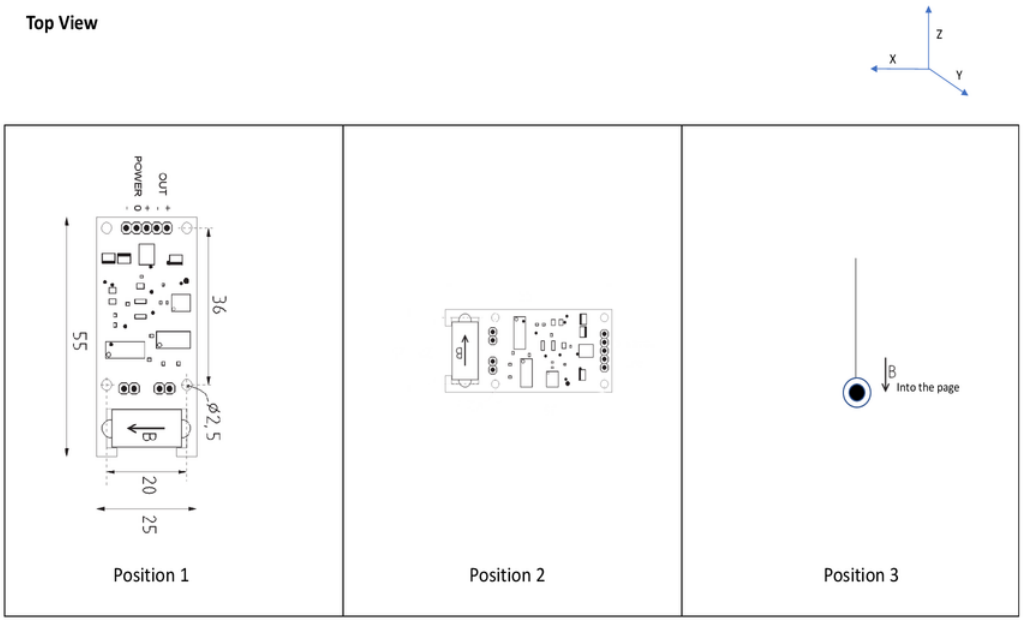

Figure 3.6: *Top down view of how the sensors were positioned during the experiments.*

be observed using a digital multimeter (DMM) and there corresponding readings collected based on the position with respect to the detection coil. It must be noted that to allow for minimal electromagnetic interference with sensor readings, all ferromagnetic materials within a 50 centimetre radius must be removed. Following this, 3 trail readings based on the orientational x-y-z axis (as seen in Figure 3.6) will be completed and the average computed and contrasted with one another. During sampling, the sensors must not be disturbed and left to complete a measurement cycle as depicted by the DMM. Earth's actual magnetic field strength is a vector quantity that can be computed and compared to the experimental orientation's resulting vector when utilising the following formula (3.4). This is important when observing if the sensor is actually sensing the earth's magnetic field or external magnetic fields caused by ferromagnetic material.

$$Earth_B = \sqrt{{x_B}^2 + {y_B}^2 + {z_B}^2} \tag{3.4}$$

Following these initial measurements, the differences in initial readings will provide the basic ground work in describing the individuality of the sensors (both sensors may be from the same company and series but they have different outputs even when replicated in the same positioning). These discrepancies must be investigated prior to amplification from the instrumental amplifiers to justify their use and exemplify the need to calibrate the sensors to the same level as a prerequisite to measurements in an operational environment.

3.5.3 Mapping Magnetic Fields in a Workspace

Other factors that must be observed when making measurements are the voltage output and corresponding magnetic field readings of the surrounding laboratory environment/ workspace to ensure that extrinsic structures such as steel supports in laboratory tables or overhead tables do not affect the measurement acquired.To achieve this, a sample space of 30cm by 30cm was set on the laboratory floor, on top of a 5 level wooden logs as shown below (Figure 3.7 and Figure 3.8) using masking tape.

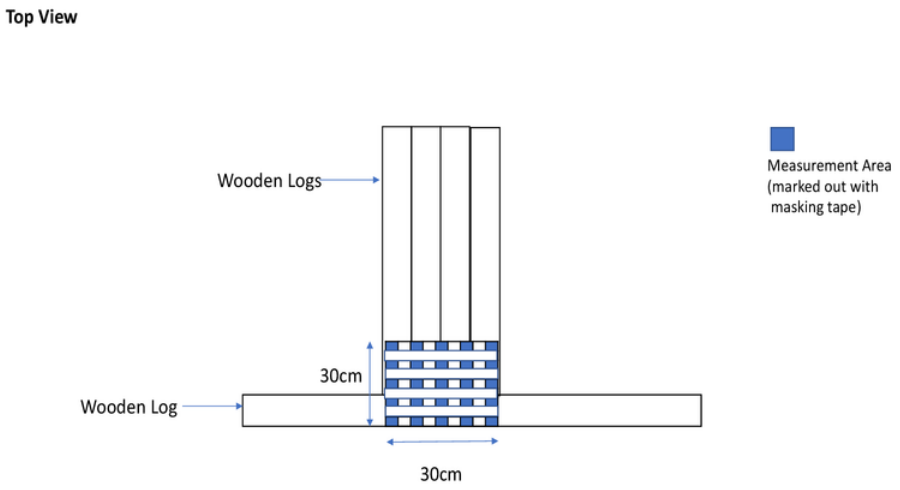

Figure 3.7: *Top down view of how the workspace was setup.*

The laboratory floor was selected due to the fact that it was easier to account for extrinsic ferromagnetic material present in the laboratory and therefore relocate to an area with fewer structures/ magnetic material around. Following this a measurement using an oscilloscope was taken every 5cm across the proposed area in the x axis and y axis to show the effects on voltage output. The sensor was also taped down using masking tape to ensure that it would be completely stationary and uniform through each measurement.

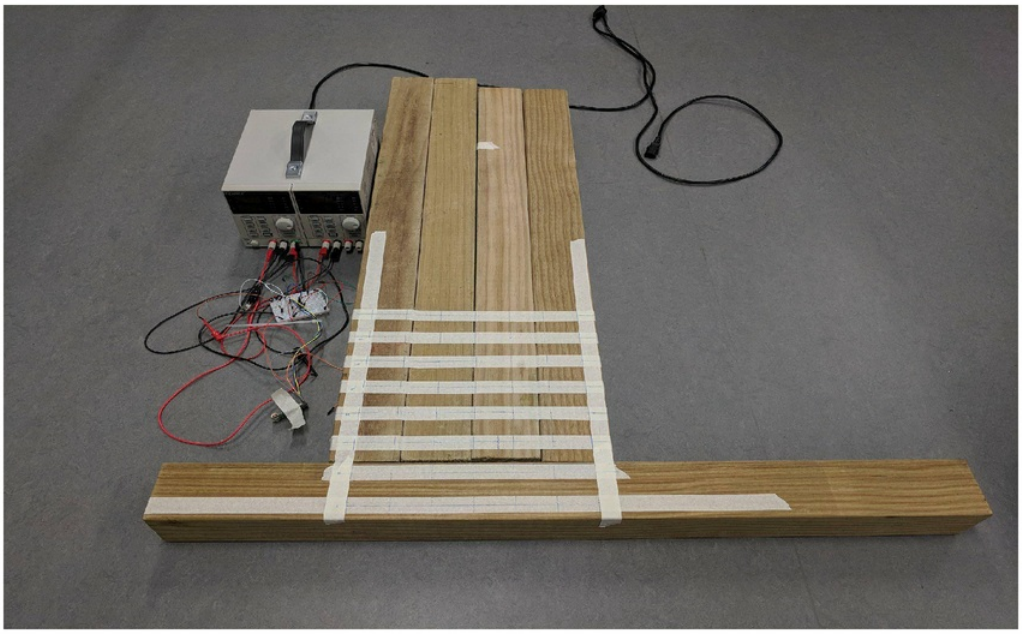

Figure 3.8: *Photograph of the experimental setup on the floor with markings on the the masking tape indicating the measurement positions required of the sensors.*

3.5.4 Sensor Susceptibility and Response to External Magnetic Fields

To identify the effects of external magnetic fields on a single sensor, each of the sensors are set within an area of the workspace at (15cm,0cm) and an initial reading is taken. To establish a frame of reference, to the right of the initial and above the initial position are considered positive, to the left and below the starting position will be considered negative. Following this, a bar magnet and subsequently a meteorite sample from the Department of Earth and Planetary Sciences were passed inline with the sensing axis/coil.This is then repeated with the external magnetic material being perpendicular to the sensing axis/coil. A photograph of the bar magnet and meteorite sample used for this experiment can be found in Figure 3.10 .

Both samples were passed from a distance of 20cm away until the material reached within 5cm of the either end or above or below the sensing axis. The bar magnet initially had the north pole facing the sensing axis and was passed across the the axis until it reached 5cm from the beginning of the coil. This was mainly due to the fact that if any material came closer than 5cm it would automatically cause the sensor to oversaturate, hence producing an output reading akin to short circuiting or at its maximum output. Also both the bar magnet and meteorite could not move any closer due to form factor and

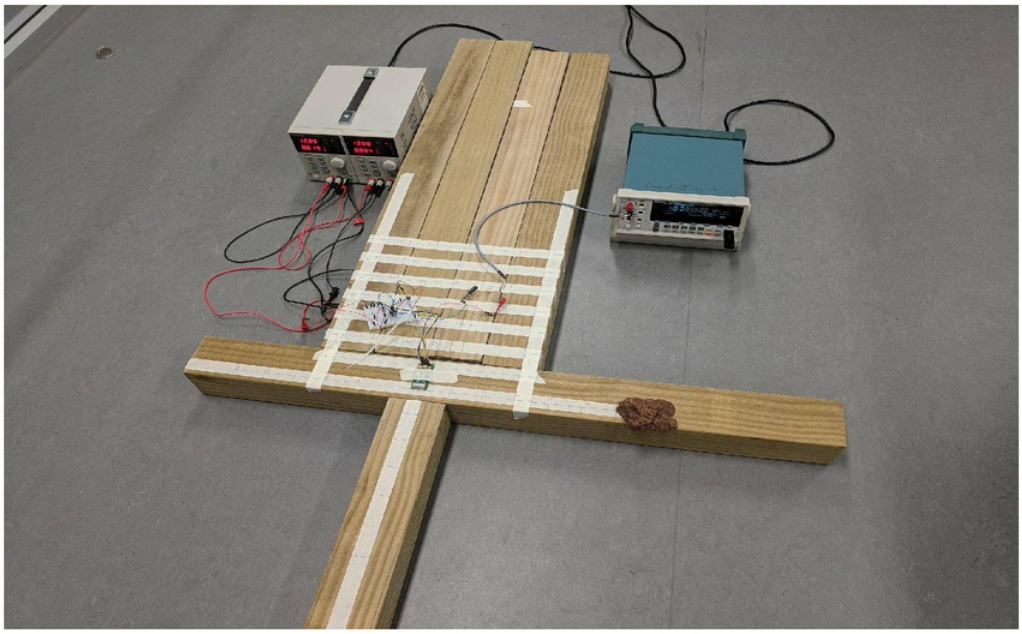

Figure 3.9: *Photograph of the sensor setup for the effects that external magnetic material have on the sensor.*

the limited space to either end of the coil. The meteorite sample was placed as shown in Figure 3.9 to imitate a meteorite flat on the ground. A 5cm position change was used each time a reading was taken. After a set of inline (right to left of the sensor's coil) readings were taken, the effects of a ferromagnetic material perpendicular (above to below) to the sensor's coil were recorded and observed. This was completed to observe how the sensor's respond if a ferromagnetic material was found outside of its standard sensing axis and provide a complete set of results detailing effects of external magnetic fields within a 20cm radius from the coil's centre.

Each measurement was taken with the default settings of the DMM and left to record a complete sample cycle before moving to the next measurement position.In doing so, it allowed the sensors to have time for the saturation levels to settle and provide a more accurate reading.The bar magnet was essentially utilised as a simulation of a strong magnet field presence and the meteorite as a relatively weak one. By observing the outputs of the sensors, the sensor's saturation level caused by an external magnetic field can be quantified and further explored when considering a dual sensor configuration.

Figure 3.10: *a)The bar magnet b)Meteorite sample utilised for this experiment.*

3.5.5 Sensor Comparison

It is important to establish that a difference between the two sensors exist before actual implementation, hence a sensor comparison is required to be performed. To accomplish this task, it was paramount to question if the sensors were affecting each other when measurements were taken or the differences in sensor output attributed to external factor (extrinsic noise or magnetic fields from unknown locations). In saying so, the results of section **3.5.1, 3.5.3** and **3.5.4** will be observed and the overall differences observed. This sensor comparison section will indefinitely complement the results from the dual sensor tests, as it identifies the existence of a difference between the two sensors, thereby legitimising the need for performing tests based on the dual sensor setup. It also validates the ability to utilise a gain to amplify the differences to present a suitable meteorite detection method.

3.6 Dual Sensor Tests

This section will describe the experimental tests completed with the dual sensor setup. It is paramount to discover if the sensors have any correlation or affect on one another when placed at different distances away and also how they respond when in use together. It is also important to identify the response the sensors display when external magnetic fields are introduced to a dual sensor setup.

3.6.1 Effects of Distance between Sensors

To accomplish this experiment, both sensors were placed parallel (sensing coils in line with each other) within the designated workspace. It is important to note that the first sensor was placed at the (0cm, 0cm) position in the workspace. The initial reading was then taken when the sensors were side by side (parallel) to each other. It was found that the sensors were roughly 2.5cm apart when placed side by side hence the second sensor was placed at (2.5cm,0). Subsequent readings were taken when the second sensor was shifted a distance of 5cm (taken from the centre of the coil) until the end of the workspace. The differences between the dual sensor outputs were then compared to the workspace readings to determine if the external magnetic fields present in the workspace were causing the differences in readings or the sensors themselves were affecting each other. This was then repeated for the three axis to further display the relationship between distance and outputted results. By observing the results of the experiment, the integral idea based on if the sensors affect each other can be established.

3.6.2 Introduction of Magnetic Field to Dual Sensor Setup

Similar to the single sensor test, the bar magnet and the meteorite sample were introduced to the system and the responses of both the sensors observed and quantified. An initial reading was taken with the sensors positioned at (0cm, 0cm) and at (17.5cm, 0cm). Following this, the bar magnet was placed 20cm away from the sensor located at (17.5cm, 0cm) and the outputs observed. The bar magnet was then moved 5cm closer to the sensor's coil per capture of the oscilloscope until it reaches 5cm from the sensor (the reason of which is stated in section **3.5.4**. A single data capture was then taken, using the 2 channel oscilloscope, with the bar magnet placed in-between both sensors. The magnet was then positioned 5cm away from the end of the sensor at (0cm, 0cm) and shifted until the magnet was 20cm from the centre of the sensor's coil. This was then repeated with the meteorite sample to contrast the response between a strong magnetic field and weak magnetic field.

3.7 Data Collection Methods

There were three main data collection methods utilised in both the single and dual sensor tests and they are as follows:

1. DMM - Tektronix DMM 4040.
2. 2 Channel Oscilloscope - Tektronix TDS2012B.
3. Arduino Uno.

For single sensor test, the DMM was utilised most of the time, due to its ability to provide accurate readings that were 6 digits long. The default capture samples were

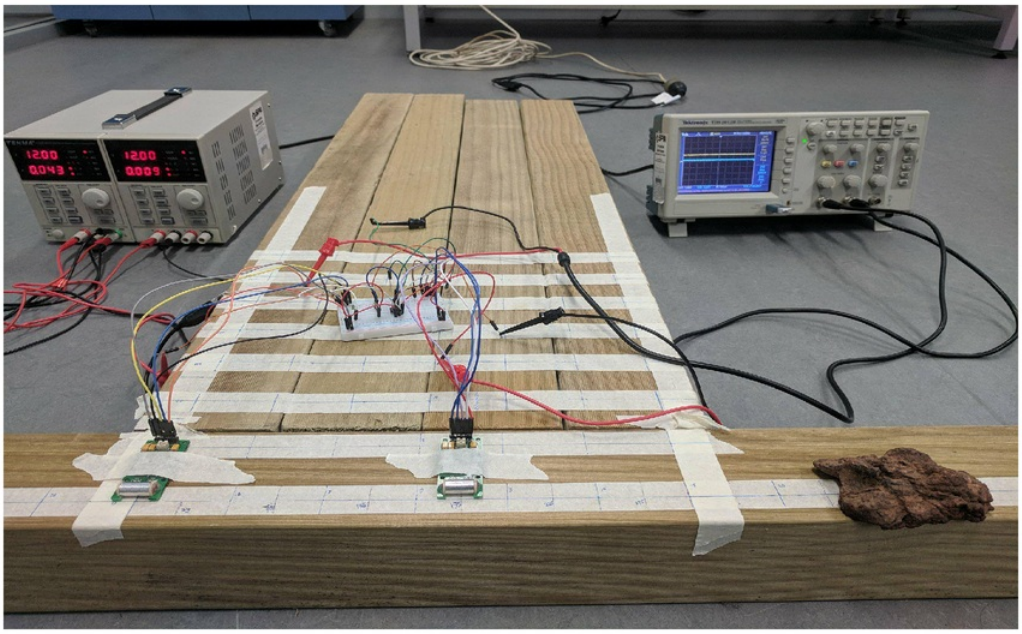

Figure 3.11: *Photograph of the sensor setup for the effects that external magnetic material have on the sensor.*

completed in either 24 or 25 seconds with 100 samples in total. Since these readings were recorded into a single csv file, it made the output readings from the sensor easy to integrate with programs such as Matlab and Microsoft Excel for post data analysis and presentation. However due to the fact that there was effectively only one measurement channel the DMM was not able to perform any of the dual sensor tests required, hence the use of the 2-channel oscilloscope. Similarly, due to the restriction on form factor when considering use in a mobile UAV, a micro-controller based design for information gathering/processing was preferred. By utilising this form of information gathering the sensor array can essentially be run with onboard battery supply and hence save a lot of room. The basic coding of the Arduino used to acquire this information can be found in (Appendix ref), however this model can be further optimised for better memory management.

Chapter 4

Results and Discussion

4.1 Single Sensor Tests

The following section displays a variety of experimental results acquired for a single sensor following the methods discussed in section **3.5.1**. It is important to note that most of these experiments are completed in a static environment and as such dynamic applications are not incorporated, hence requiring further investigation.These dynamic tests include such things as sampling rate of the sensors and optimal speed for the UAV to travel. Sampling rate is an important factor that should be addressed, however due to time constraints could not be explored and would require further investigation. Similarly, the optimal speed for the UAV would also have to be further investigated due to the sensors being different to prior research.

4.1.1 Initial Sensor Calibration

There were two methods that were trailed to produce a level system and account for the zero drift characteristic in both sensor outputs. The first involved the use of a resistance turnpot/trimpot (potentiometer) as a physical mechanism, similar to a voltage divider, allowing the initial readings to be levelled out and provide a suitable base for future measurements. The other method involved adding a resistor before the inputs on sensor 1 limiting the input to a value just below 12V to imitate a level system. This method however, would not function as the sensors would not be functioning to their full capabilities due to the voltage limitation.

In a dynamic/realistic environment, both methods are considered obsolete due to the fact that every change in position quantifies a change in the corresponding outputs and initial readings. Essentially, this results in the system requiring constant adjustment through increasing or decreasing resistance in order to create a level measurement base. This can not be completed in a closed system as it requires the turnpot/trimpot or voltage dividing circuit to be adjusted or replaced whenever the UAV travels or sensor suite shifts it's position. As a result, both methods are not advisable for use in a realistic environment.

Therefore, it is must more efficient to leave the initial reading as they stand and just

record the difference and compare this when an ferromagnetic material is introduced. This is mainly due to the fact that the expected difference when an external magnetic field is applied would no doubt be larger than the initial difference and therefore make the material noticeable through this acquired difference. Arduino would be the preferred method of collecting this data but to do this it would require additional coding and further research in order to produce a system with minimal data loss.

4.1.2 Directional Response

It can be seen from the figures below (Figure 4.1, 4.2 and 4.3) that an offset from zero exists on all 3 axis orientations even when there is no applied external magnetic field. For all 3 axis, sensor 1 seems to output a higher voltage when compared to the output of sensor 2. These output differences provide a suitable difference that can be amplified by the instrumental operational amplifier.

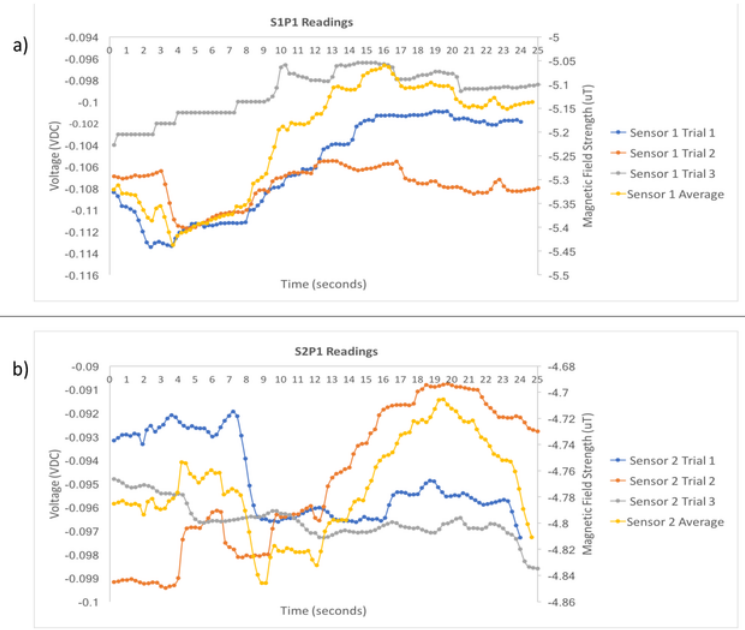

Figure 4.1: *Sensor data acquired for position 1 using a DMM following the experimental setup as described in 3.5.2. a) Sensor 1 readings acquired after 3 trails were performed and the associated average, alongside the equivalent magnetic field strength as measured in micro Teslas. b) Sensor 2 readings following the method as sensor 1. When observing readings for position 1 it is revealed that the average output of sensor 1 is greater than sensor 2 by approximately 0.0089V or 0.444μT.*

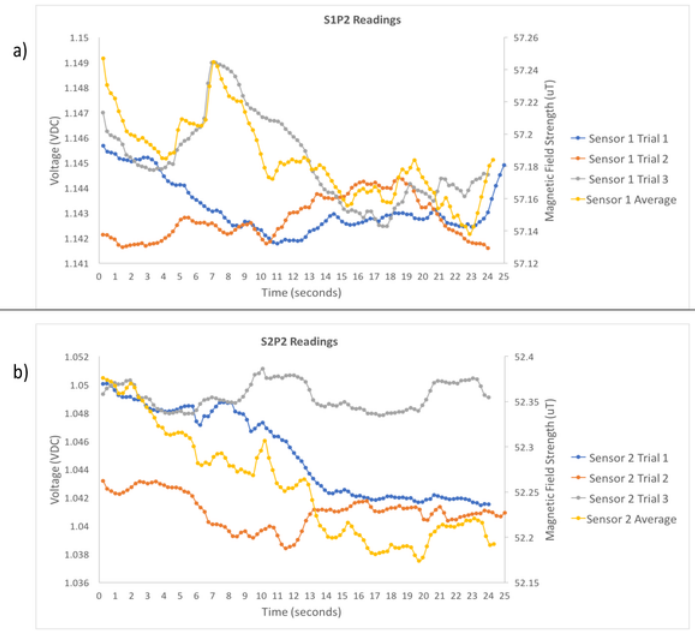

Figure 4.2: *Sensor data acquired for position 2 using a DMM following the experimental setup as described in 3.5.2. a) Sensor 1 readings acquired after 3 trails were performed and the associated average, alongside the equivalent magnetic field strength as measured in micro Teslas. b) Sensor 2 readings following the method as sensor 1. When observing readings in position 2 it is revealed that the average output of sensor 1 is greater than sensor 2 by approximately 0.099V or 4.929μT.*

Figure 4.1 and Figure 4.3 displays the ability of the sensors to output a negative measurement and subsequently the need for an inverting operational amplifier. By applying an inverting op-amp, the sensor outputs can become acquired by the Arduino and hence provide an accurate difference reading. Table 4.1 surmises the findings and differences between the sensor outputs. The voltage to tesla conversion was completed following the FL1-500 characteristics as 0.02V coverts to 1μT. It is important to note the vector positions as the two outputs should theoretically be proportional to Earth's magnetic field strength. However, by acquiring the co-ordinates of Macquarie University (-33°46'30.93" S 151°06'46.49" E [16]) and cross referencing that with the 2015 Australian government's geomagnetic reference field computation [10], it was found the total field strength was equal to 57052 nT or 57.052 μT. This result was computed by a similar method with the three standard axis x-y-z with the only difference being the inclusion of a magnetic inclination (angle between magnetic field and horizontal plane) and declination component

Table 4.1: Directional test summary in terms of average output over 3 trails (3 d.p.).

	P1	P2	P3	Vector Position
Sensor 1 (V)	-0.104	1.144	-4.449	4.595
Sensor 1 (μT)	**-5.187**	**57.185**	**-222.472**	**229.762**
Sensor 2 (V)	-0.095	1.045	-4.184	4.313
Sensor 2 (μT)	**-4.773**	**52.256**	**-209.192**	**215.673**

Figure 4.3: *Sensor data acquired for position 3 using a DMM following the experimental setup as described in 3.5.2. a) Sensor 1 readings acquired after 3 trails were performed and the associated average, alongside the equivalent magnetic field strength as measured in micro Teslas. b) Sensor 2 readings following the method as sensor 1. When observing readings in position 3 it is revealed that the average output of sensor 1 is greater than sensor 2 by approximately 0.266V or 13.279μT.*

(angle between horizontal plane and true north) as shown in 4.4.The Australian government's geomagnetic reference field computation is only completed every 5 years [10] so this was the newest data available based on the co-ordinates.

When comparing the experimental values obtained from both sensors to the one provided by the Australian government, it can be observed that the sensor outputs are approximately 3.5 to 3.7 times larger. The reason pertaining to this difference is not really known but it is speculated that, it is caused by all the surrounding external magnetic fields

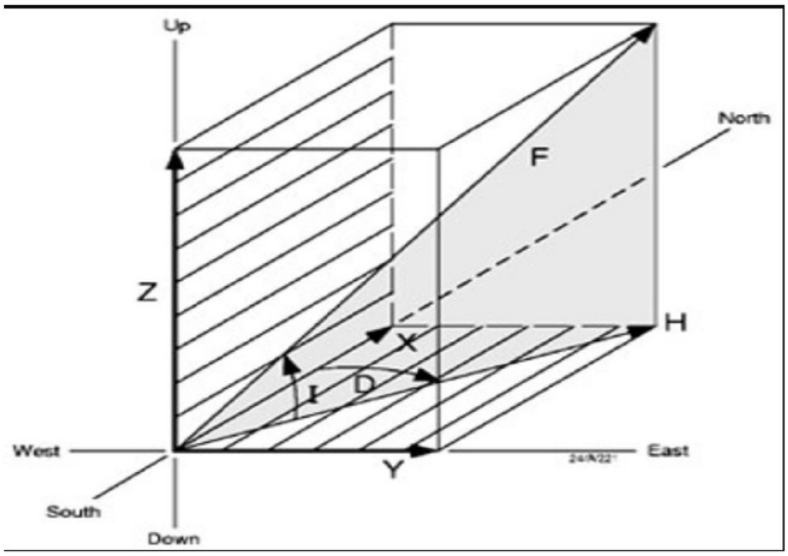

Figure 4.4: *How the theoretical vector value of Earth's Magnetic Field was determined [10].*

permeating from the floor or electrical devices such as power supply, DMM/oscilloscope, overhead lights etc.

4.1.3 Mapping Magnetic Fields in a Workspace

In theory, the magnetic field strength in an ideal environment (with no external magnetic field sources or without any noise) should be the same across any workspace area and proportional to a vector measurement of the Earth's magnetic field. However, as it can be seen in Figures 4.5, 4.6 and 4.7 the magnetic field strength, as recored by each sensor, exhibits a change in the sensor's output as it was moved across the sample space. To produce accurate readings, it is advised that the workspace provides close to ideal conditions. However, the graphical representation of the measurements were the best representation of the sensor's saturation levels in a laboratory environment. It can be concluded that the sensors response in all three positions resulted in an anisotropic readings (any shift in the sensors position resulted in a corresponding shift in the voltage/magnetic field strength output). For future reference, it is advised that instead of a laboratory environment, the environment that the sensor suite was intended to be utilised in should be selected and a workspace measurement completed in said environment. This being stated the results of this experiment are still useful as a referencing point when conducting the same test with a dual sensor setup in a laboratory environment.

By acquiring the readings by position increment, it was also possible to calculate the

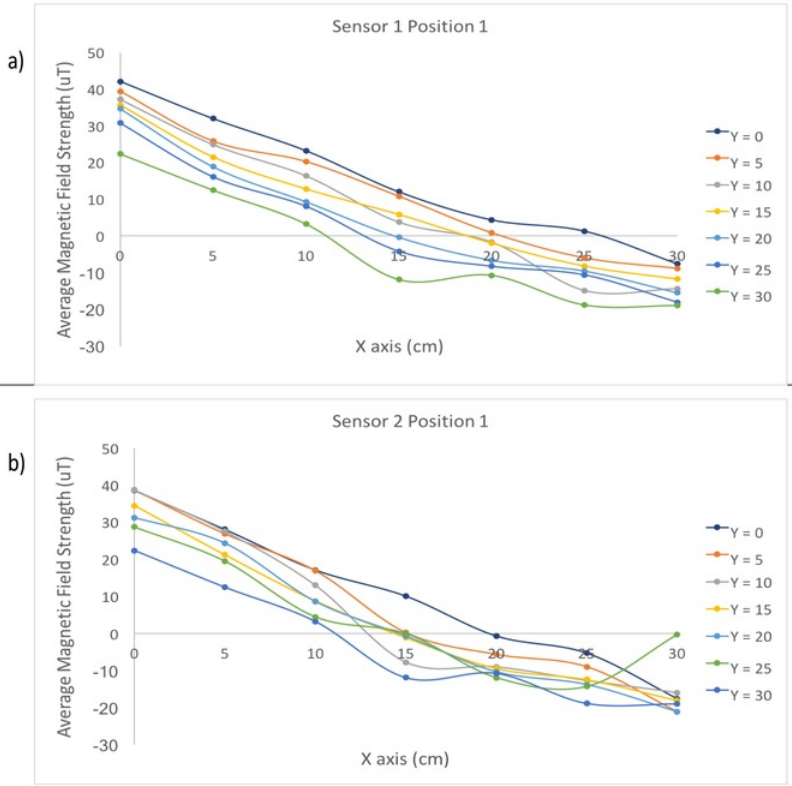

Figure 4.5: *Average magnetic fields (μT) mapped in the allocated 30cm by 30cm workspace as acquired in position 1 a) Sensor 1 readings with incremental readings of 5cm until the limits of the workspace were reached. On average the each move resulted in a magnetic difference of 8.109 μT. b) Sensor 2 readings 1 with incremental readings of 5cm until the limits of the workspace were reached. On average the each move resulted in a magnetic difference of 8.954 μT.*

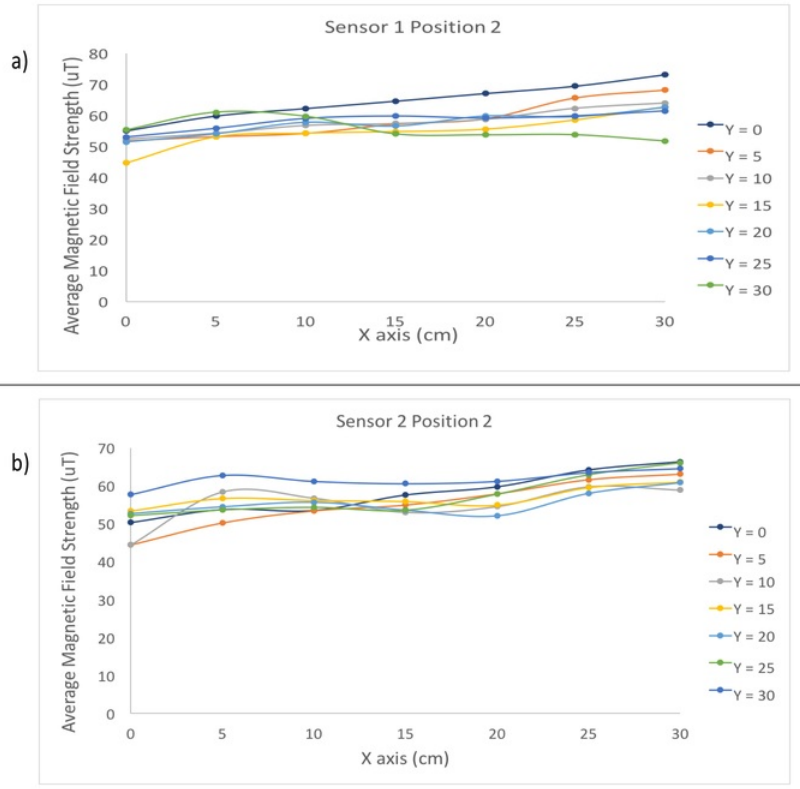

Figure 4.6: *Average magnetic fields (μT) mapped in the allocated 30cm by 30cm workspace as acquired in position 2 a) Sensor 1 readings with incremental readings of 5cm until the limits of the workspace were reached. On average the each move resulted in a magnetic difference of 2.442 μT. b) Sensor 2 readings 1 with incremental readings of 5cm until the limits of the workspace were reached. On average the each move resulted in a magnetic difference of 2.740 μT.*

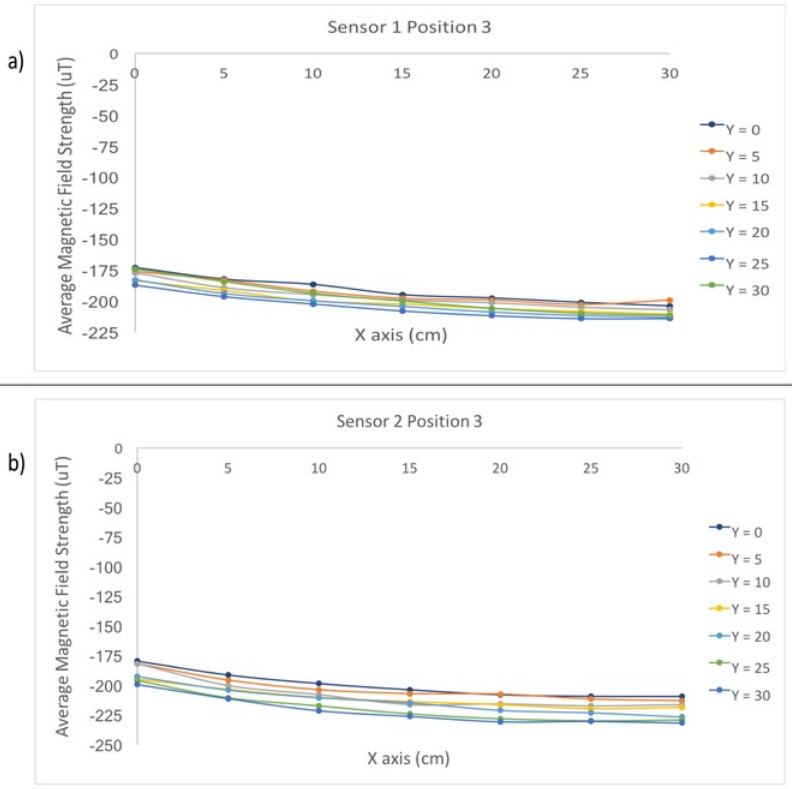

Figure 4.7: *Average magnetic fields (μT) mapped in the allocated 30cm by 30cm workspace as acquired in position 3 a) Sensor 1 readings with incremental readings of 5cm until the limits of the workspace were reached. On average the each move resulted in a magnetic difference of 5.053 μT. b) Sensor 2 readings 1 with incremental readings of 5cm until the limits of the workspace were reached. On average the each move resulted in a magnetic difference of 5.378 μT.*

corresponding difference between each move and as such acquire the magnetic gradient per position. The magnetic gradient is the difference in magnitude of a magnetic field H or magnetic flux B with respect to the change of distance between two points and is calculated by:

$$\frac{\Delta B}{\Delta d} \tag{4.1}$$

By utilising the above equation the magnetic gradient of the different positions can be acquired and are displayed in Table 4.2.

Table 4.2: Workspace Magnetic Gradient as recorded per position

	Sensor 1	Sensor 2
P1	1.622	1.791
P2	0.488	0.548
P3	1.011	1.076

It is important to understand that the magnetic gradient of the sensor suite represents the field gradients produced by magnetic anomalies as by, keeping the distance constant any large change in the measured magnetic field strength will indicate the presence of ferromagnetic material. This being stated the gradient should be constant as the only factor that varies is the measured magnetic field and in an ideal environment the magnetic field is constant. However, in the case of the above readings the gradient per position can be seen to be varying hence leading to the conclusion that there exists some ferromagnetic sources within the laboratory that can skewer the results.

4.1.4 Sensor Susceptibility and Response to External Magnetic Fields

Both sensor's responses to the bar magnet and meteorite sample can be found in Figures 4.8 and 4.9. Theoretically, the sensors should have a similar response when the same magnet is material present. However, for both they exhibit anisotropic magnetic field responses depending on material and magnetic orientation (inline or perpendicular). The inline orientation would have the highest measured average magnetic field reading as the ferromagnetic material approaches either end of the sensing coil. This is in congruent with the measured responses as both sensor 1 and sensor 2 display a large magnetic field output at 5cm away from either sides of the coil and a more muted response as the material is placed away from the sensors and formula 2.1 from background knowledge. The average magnetic field strength responses are however never to reach 0 due to the residue external magnetic fields present in the laboratory and also due to the Earth's natural magnetic field as can be seen in the presence of both magnetic material.

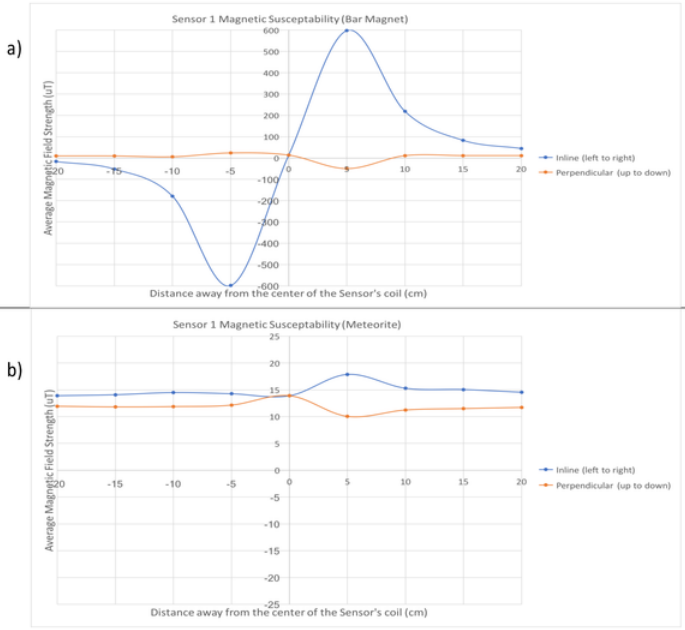

Figure 4.8: *Measured response from the sensor 1 when an external magnetic field is applied. a) Response from a relatively strong magnetic presence, in the form of a bar magnet. b) Response from a relatively weak magnetic material in the form of the meteorite sample. Both samples are separated according to orientation (inline or parallel).*

This being stated, for the the perpendicular readings, theoretically the output should be the largest as the material passed the centre of the coil but from both sensor response's it can be shown that a comparatively small change exists as the material gets closer. Only when the material reaches roughly 5 cm away from the centre of the coil can a significant influence on the output be observed. This establishes that the sensor's are the most sensitive when a ferromagnetic material is placed inline with its measurement/sensing axis. In both sensor tests, the maximum difference between the average magnetic field strength in all positions occur at 5cm away from the beginning of the coil or end of the coil and with the north face of the magnet either end. Table 4.3 highlights some of the main observations from the experiment:

To further improve on the reliability of the results and experimental method would require the sensor to be mounted and have the sample be passed under the sensor to imitate the sensor suite travelling over a ferromagnetic material . This not only results in the sensor suite application more relatable to its operational environment but also allows for readings closer than 5cm to be taken. Furthermore it would be more efficient

Table 4.3: Summarisation on the measurements made in conjunction to both sensor's susceptibility to external magnetic fields.

Bar Magnet (Strong Magnetic Field)		
	Sensor 1	Sensor 2
Initial Average Reading (V)	0.268	0.120
Initial Average Reading (μT)	13.381	5.996
Maximum Average Reading (V)	at (-5,0) = -11.959	at (-5,0) = -11.969
Maximum Average Reading (μT)	597.440	578.624
Maximum Average Difference (μT)	between (0,0) and (-5,0) = 611.319	between (0,0) and (-5,0) = 604.462
Meteorite Sample (Weak Magnetic Field)		
Initial Average Reading (V)	0.278	0.065
Initial Average Reading (μT)	13.391	3.27
Maximum Average Reading (V)	at (+5,0) = 0.358	at (-5,0) = 0.120
Maximum Average Reading (μT)	597.440	578.624
Maximum Average Difference (μT)	between (0,0) and (+5,0) = 584.058	between (0,0) and (+5,0) = 572.628

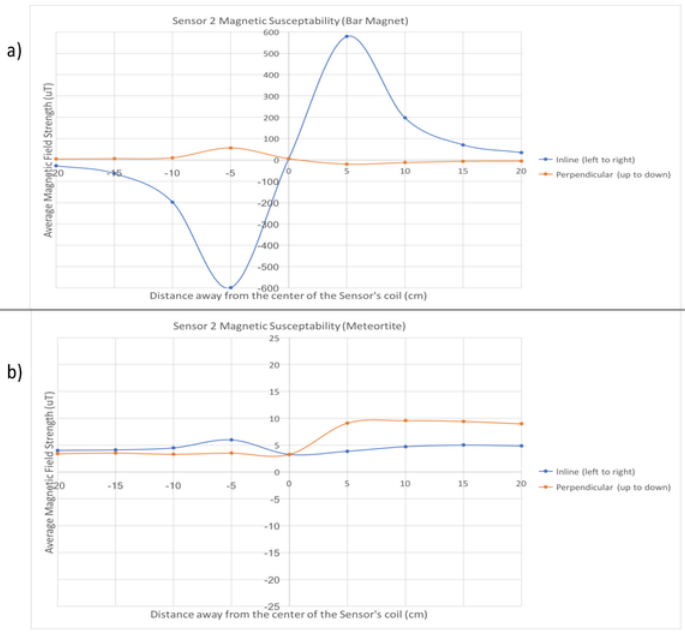

Figure 4.9: *Measured response from the sensor 2 when an external magnetic field is applied. a) Response from a relatively strong magnetic presence, in the form of a bar magnet. b) Response from a relatively weak magnetic material in the form of the meteorite sample. Both samples are separated according to orientation (inline or parallel).*

to have shielded wiring to prevent any external magnetic fields from interacting with the sensors when undergoing measurements.Though, the current method is able to establish an simplistic relationship between distance from the ferromagnetic material in most radial distances from the centre of the coil.

In a realistic environment, the outputs of the sensors will rarely reach that high of an output as described in the case where a strong magnetic field is administrated but will largely exhibit a similar pattern as shown in the weaker magnetic field response. Due to this fact, an Arduino Uno micro-controller can be used as mobile data storage as the highest exhibited voltage output under the influence of the meteorite sample was 0.358V and that is well within the sensing range of the Arduino. It is wise to apply a gain to ensure all data readings can be acquired due to these small readings though and this can be achieved by the instrumental amplifiers as shown in Figure 3.5 in Section 3.4 (circuit diagram).

4.1.5 Sensor Comparison

In a laboratory environment the sensors exhibit varying results that lead to the following conclusions:

- Sensor 1 generally outputs a larger average voltage and therefore larger average magnetic field strength than sensor 2. However, both sensor's output a vector total average magnetic field strength that is 3.5 to 3.7 times larger than the theoretical value. This can attributed to the presence of external magnetic fields present in the laboratory resulting in the conclusion that a workspace in the sensor's operational environment is preferred when completing any form of measurement involving these sensors.

- Similar outputs are acquired across the workspace for both sensors, with a relationship between the change in position resulting in a change in output. When observing the graphed results though, in most cases sensor 2 exhibits a larger variance in average magnetic field strength over the various positions and as a result, has a magnet gradient that is generally greater then that of sensor 1. In an ideal environment this should not occur as the magnetic field of the external environment should be minimal with the sensor only outputting a response proportional to Earth's magnetic field.

- Both sensors are relatively sensitive when a ferromagnetic material is introduced, however this is much more evident when observing the response of the sensor's when a strong magnetic field presence is placed within a 20cm radius of the centre of coil and inline with the sensor's sensing axis. At a distance of 5cm from the centre of the coil under a strong magnetic field both sensors output close to their maximum output and it is not until roughly 15cm away that the sensor's saturation levels become relatively stable. The response to a perpendicular field in both weak and strong presences result in minute changes and it is not until the sample is within 5cm that any change can be seen in the sensor's output. These findings can be considered congruent with theoretical results as the closer the material is the stronger the measured field response.

4.2 Dual Sensor Tests

This section will detail the results from a dual sensor setup. Essentially this dual setup represents a gradiometer suite as the difference accosted from the sensor outputs acts as the main detection method for ferromagnetic material. Similar to the single sensor tests, these corresponding results will be completed in a static environment and within the defined workspace laboratory environment. To further solidify the functionality of this setup the first agenda will involve providing an answer as to whether the sensors effect each other when considering the distance between them. The second agenda involves the identification of the how external magnetic fields impact the dual sensor setup. By observing both these outputs, it will provide a in-depth insight as to the usefulness of the FL1-500 sensors as the sensors of choice in a drag-line orientated sensor suite.

4.2.1 Effects of Distance between Sensors

The corresponding oscilloscope graphs that display the voltage output when one sensor has it's position changed by 5cm each measurement cycle and with minimal noise from external sources of magnetic fields can be found in Appendix A.1 . For this set of results, sensor 1 is left stationary by taping the sensor down with masking tape and sensor 2 is shifted. It is apparent when observing the single sensor mapping of the workspace that each position change results in a different output. This is congruent with the data acquired with a dual sensor setup as in all three sensor orientations, sensor 2 is shown to output a varying voltage with every move. This is further exemplified when comparing the average magnetic field changes for the workspace and the output of sensor 2 or channel 2 as the sensor has it's position shifted.

For P1, the change in average magnetic field strength of sensor 2 in the workspace environment was found to be 8.954 μT and for a dual setup, 9.385μT. The difference is relatively small at 0.431μT between the two setups. P2, seems to be an outlier with the change in average magnetic field strength of sensor 2 recorded as 3.693 μT as compared to 9.938 μT of the dual setup, resulting in a difference of 6.245 μT. P3 also has a similar difference with 3.353 μT. From observing all these difference it can be shown that the presence of another sensor does seem to affect the readings with only P1 displaying a small variance in the difference between workspace and dual sensor setups. This is also shown when observing the changes with sensor 1. Because sensor 1 is stationary, theoretically the sensor should provide a constant average magnetic field but in all three position readings, sensor 1 also displays a difference as shown in Table 4.4 as sensor 2 is moved away. Hence, revealing that the sensors do in fact affect each other, so as a result is it important to establish a optimal distance between the two sensors (centre of measurement coil to centre of measurement coil) where they will have minimal affect on each other's readings but also some correlation between the two sensors. This correlation allows the sensors to function as a gradiometric fluxgate magnetometer and not just two individual sensors (which defeats the point of having a dual sensor array).

Table 4.4: Summary of outputs for all three positions in a dual sensor setup.

P1				
Position S1 (cm)|S2(cm)	**Average S1 Output (μT)**	**Average S2 Output (μT)**	**ΔS1 Output (μT)**	**ΔS2 Output (μT)**
(0,0)|(2.5,0)	44.865	53.890	-	-
(0,0)|(7.5,0)	45.643	36.890	0.778	17
(0,0)|(12.5,0)	47.42	17.675	1.777	19.215
(0,0)|(17.5,0)	47.956	9.2776	0.536	8.398
(0,0)|(22.5,0)	48.626	0.9632	0.6704	8.3144
(0,0)|(27.5,0)	49.452	-0.0484	0.826	3.385
-	-	**Average Total Δ**	**0.917**	**9.385**
P2				
Position S1 (cm)|S2(cm)	**Average S1 Output (μT)**	**Average S2 Output (μT)**	**ΔS1 Output (μT)**	**ΔS2 Output (μT)**
0,0)|(0,2.5)	51.070	42.208	-	-
(0,0)|(0,7.5)	56.082	56.290	5.0128	14.0824
(0,0)|(0,12.5)	53.681	63.268	2.402	6.978
(0,0)|(0,17.5)	49.926	63.790	3.755	0.522
(0,0)|(0,22.5)	57.854	0.963	7.928	62.826
(0,0)|(0,27.5)	49.452	-0.0484	8.4016	3.385
-	-	**Average Total Δ**	**5.500**	**9.938**
P3				
Position S1 (cm)|S2(cm)	**Average S1 Output (μT)**	**Average S2 Output (μT)**	**ΔS1 Output (μT)**	**ΔS2 Output (μT)**
(0,0)|(2.5,0)	-186.868	-190.748	-	-
(0,0)|(7.5,0)	-178.972	-199.216	7.896	8.468
(0,0)|(12.5,0)	-179.628	-200.444	0.656	1.228
(0,0)|(17.5,0)	-179.056	-202.488	0.572	2.044
(0,0)|(22.5,0)	-179.416	-206.26	0.36	3.772
(0,0)|(27.5,0)	-180.056	-191.652	0.64	14.608
-	-	**Average Total Δ**	**2.025**	**8.468**

Due to the limited space available to create a portable dragline sensor for a UAV, it is important that the optimal distance between the two senors not be too large as this would affect the small form factor of the sensor array. From the results shown in Table 4.4, a suitable distance that could be selected is around 17.5cm to 20cm apart. This is due to the fact that at approximately 17.5cm apart, the orientational data exhibits one of the smallest changes in between the previous reading at 12.5cm and the next reading

at 22.5cm, hence portraying the distance as just on the verge of being unaffected by each other but also has with a small lingering affect still present.

4.2.2 Introduction of Magnetic Field to Dual Sensor Setup

Similar to section **4.1.4**, this portion of the results aims to show the effects of a relatively strong and weak magnetic field on a dual sensor suite. As a result, of identifying that the sensors are most sensitive with an inline setup, the results would only include readings for both ferromagnetic material in an inline setup. The oscilloscope results can be found in Appendix A.2. These results can be improved upon if the accuracy of the oscilloscope could be increased to accomodate the relatively small output changes present when a weak external magnetic field is applied.

When a strong magnetic field is applied (bar magnet), the outputted results is congruent with theory as both sensors output smaller voltages and therefore magnetic field measurements the further the material is away. What is of interest is how the sensor behaves when the material gets to the middle of the suite. As the material enters the middle portion of the suite the outputs of both sensors are relatively high as seen by the resulting outputs at approximately 8cm although sensor 1's output drops faster, an obtainable difference can be seen. It is from this difference that the suite will be able to discern the presence of a ferromagnetic material. The maximum obtainable difference in the sensor suite's output

Realistically though, the outputs of the sensor suite will be similar to that as displayed in Figure 4.11. As the meteorite reached the centre of the dual sensor setup, sensor 1's output did not vary a lot and instead sensor 2's output dropped hence producing a noticeable difference. This being stated when utilising the oscilloscope to acquire this data , the measurements displayed in the changes in the graphs (Appendix A.1) were not noticeable. Only when the complete csv, file was a sensible reading obtainable. For further tests with the dual sensor setup it would be advisable to use a capture device with more sensitivity and therefore resolution in order to capture all the small variations in output that the sensor's may display.

This being stated it is fair to conclude that the FL1-500 can be utilised instead of the FLC-100s in the design of the dragline sensor. However, more tests would have to be performed in an environment with minimal external magnetic fields present or in the sensor suite's intended environment. It is also plausible to capture the data using a microprocessor such as the Arduino Uno but further research would have to be completed before that can be considered.

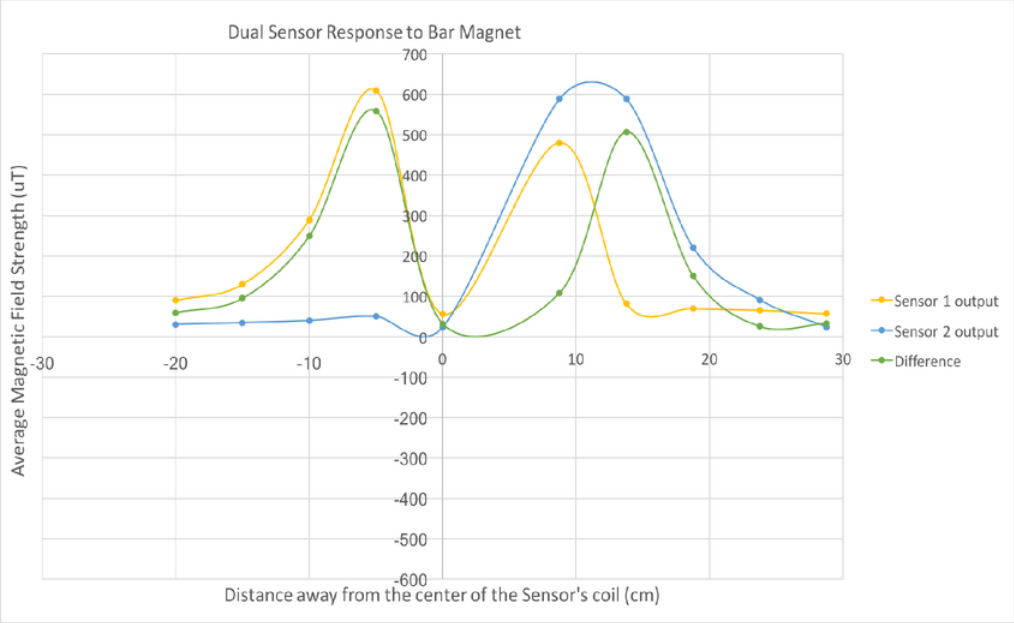

Figure 4.10: *A noticeable difference can be acquired when utilising the results from the oscilloscope. By converting the voltage output to a magnetic field, the output of the above difference can be calculated and quantified.*

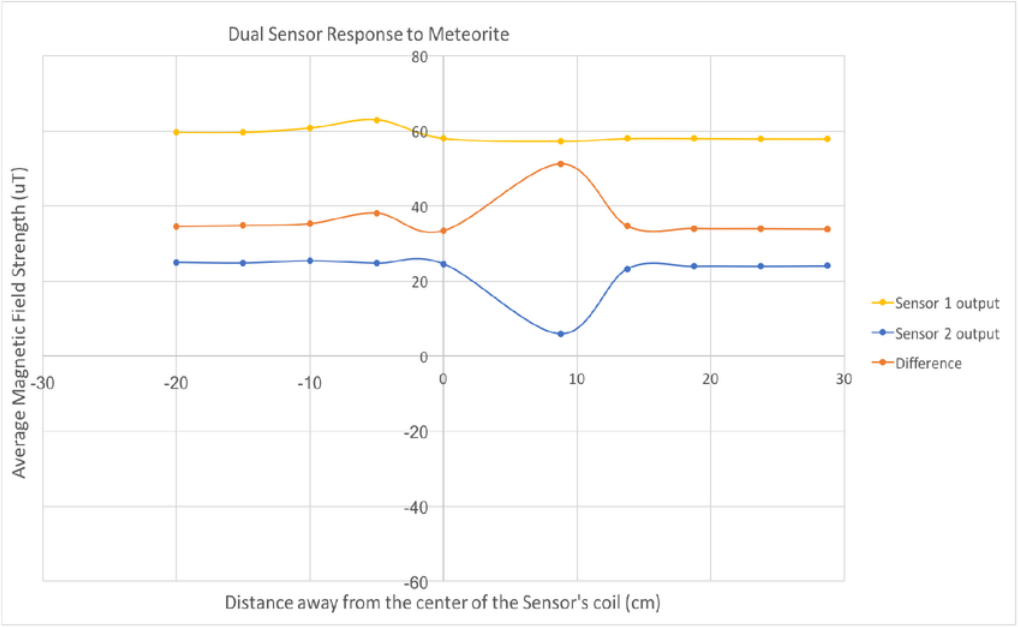

Figure 4.11: *The dual sensor's response to the meteorite sample is relatively harder to characterise with the oscilloscope readings and hence the resulting graphs do not display an difference that is as clear as with the magnetic response with a bar magnet.*

Chapter 5

Conclusions and Future Work

This thesis has provided the starting point for future research into a dual sensor dragline suite and its subsequent use in conjunction with a UAV. This being stated, this sensor array design can be paramount to aid in the search for meteorites and other faint magnetic fields and would undoubtably increase the coverage for a UAV and reduce human resources. By completing this research, a comprehensive sensor suite could be prototyped however there were many set backs preventing this from occurring.

A key component of this overall project involved the testing of a pair of Stefan Mayer FL1-500 sensors and providing a clear answer as to whether these sensors were applicable to the drag-line configured sensor suite. To accomplish this, a variety of experiments were completed and by exploring the sensor's individual functionality and characteristics it was established that the sensors were indeed suitable for use in a dragline configurations. These experiments ranged from the sensor's individual response to both weak and strong magnetic fields to response of both sensors when used in tandem to sense weak and strong magnetic fields. This being stated, prior research was conducted with a similar sensor but in boom orientation, which lead to the conclusion that a dragline orientation is more suited for meteorite discovery.

The results of the experiments revealed that the sensors were relatively sensitive to external sources and in order to reduce these effects on the sensors, it is advised that the experiments be completed in a noise free environment. The presence of external noise impacted the sensors to such a degree that even when there was no ferromagnetic material within the vicinity of the sensor's measurement coil, the sensor would output a voltage corresponding to 3.5-3.7 times that of Earth's magnetic field. So, in order to reduce these effect it would be important to place the sensor suite in nature or in a place where the surrounding magnetic field strengths can be quantified and accounted for. When used in tandem with each other a dual sensor setup presented a useful difference output that could be utilised in detecting meteorites. However, this model will have to be further refined to identify the true capabilities of the model.

In the future it is entirely plausible for the suite to be prototyped with the findings in this thesis as base. This being stated, a lot more investigation would need to be completed before this occurs. These investigations would include the full implementation

alongside a micro-controller to make the suite portable for use in UAV applications and also integration and also how the sensor suite responds in any environment with a lot of external magnetic fields of varying strengths and how to isolate the readings in such environments.

Appendix A

Oscilloscope Readings

A.1 Results for 4.2.1

The following graphs represent the results taken from the oscilloscope for section 4.2.1.

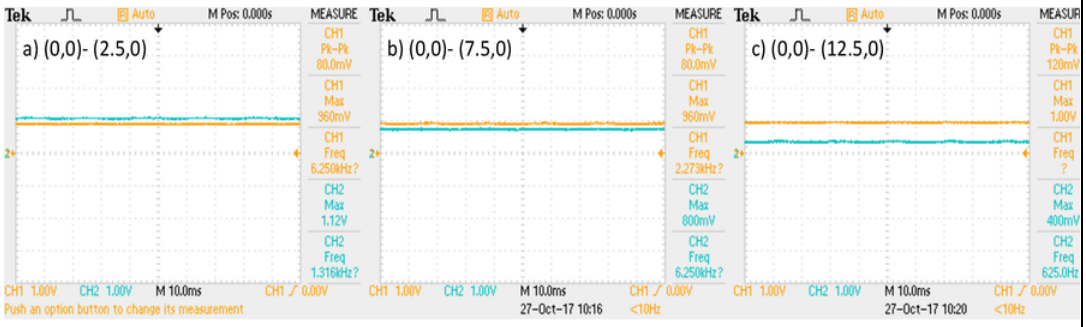

Figure A.1: *The data acquired from P1 indicates the effects on the voltage output of the dual sensor setup as the position is changed by 5cm per reading. Channel 1 represents readings from sensor 1 and channel 2 represents readings from sensor 2.*

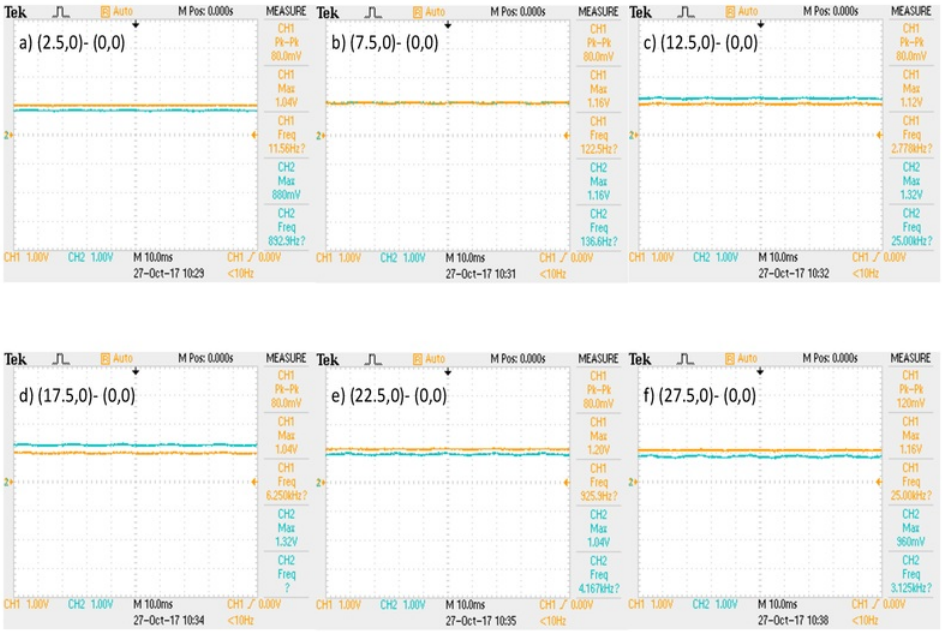

Figure A.2: *The data acquired from P2 indicates the effects on the voltage output of the dual sensor setup as the position is changed by 5cm per reading. Channel 1 represents readings from sensor 1 and channel 2 represents readings from sensor 2.*

A.2 Results for 4.2.2

The following graphs represent the results taken from the oscilloscope for section 4.2.2.

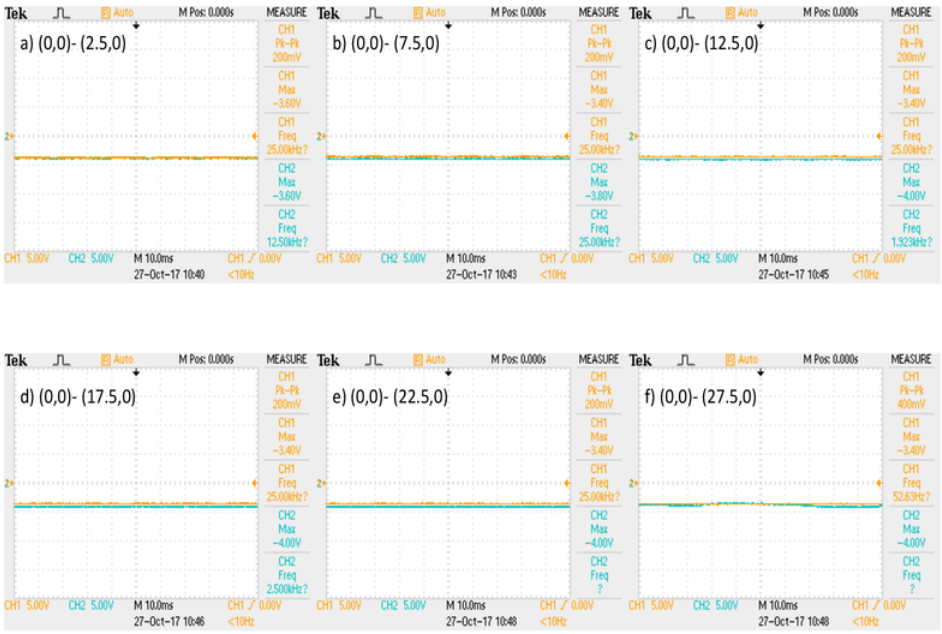

Figure A.3: *The data acquired from P3 indicates the effects on the voltage output of the dual sensor setup as the position is changed by 5cm per reading. Channel 1 represents readings from sensor 1 and channel 2 represents readings from sensor 3.*

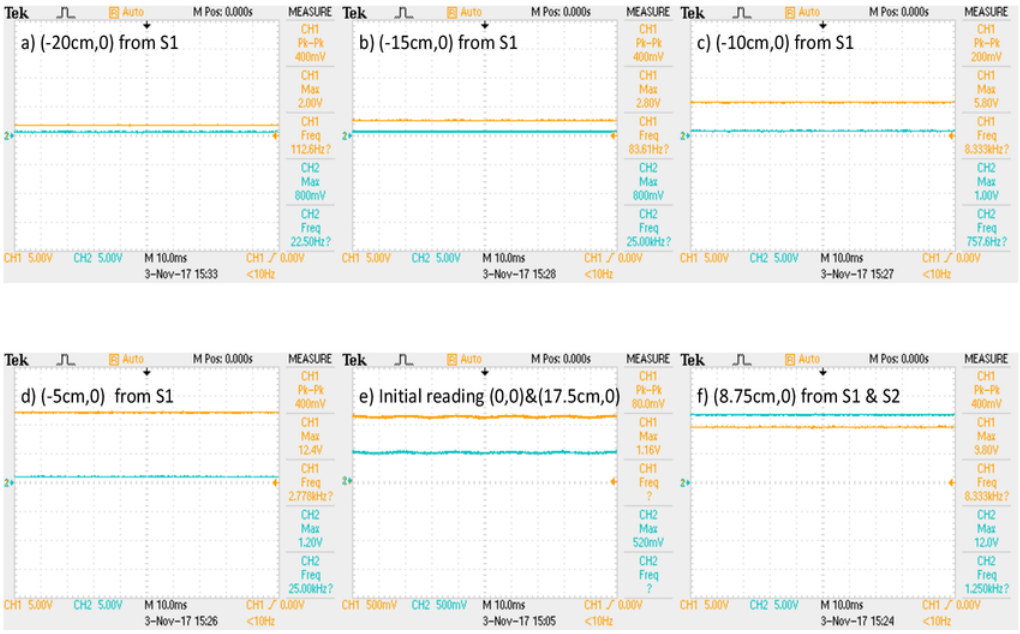

Figure A.4: *Oscilloscope readings as the bar magnet is passed inline with the dual sensor setup.*

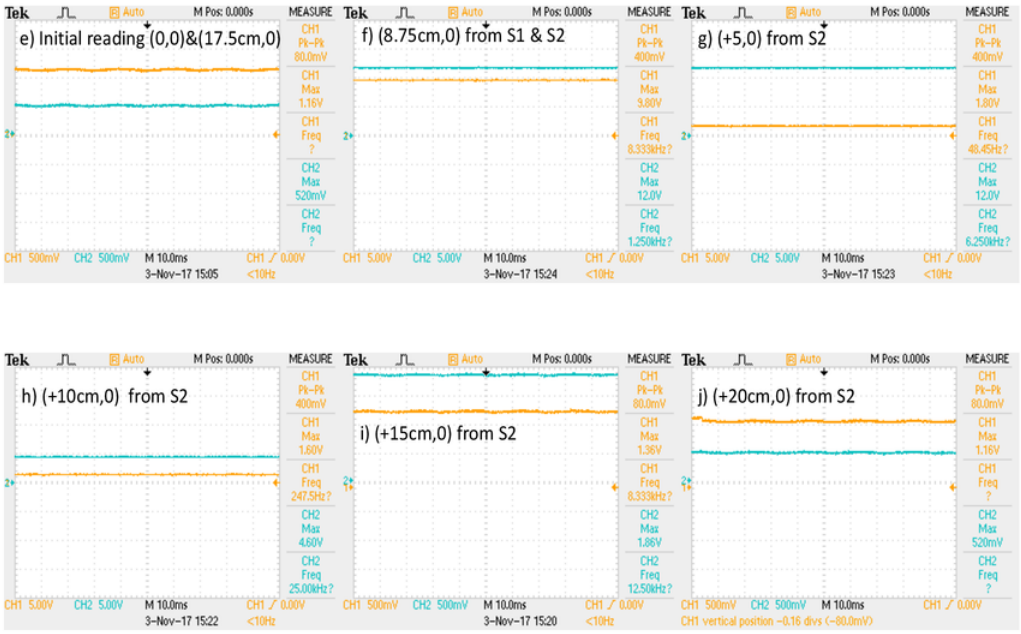

Figure A.5: *Oscilloscope recording as the bar magnet is passed inline with the dual sensor setup.*

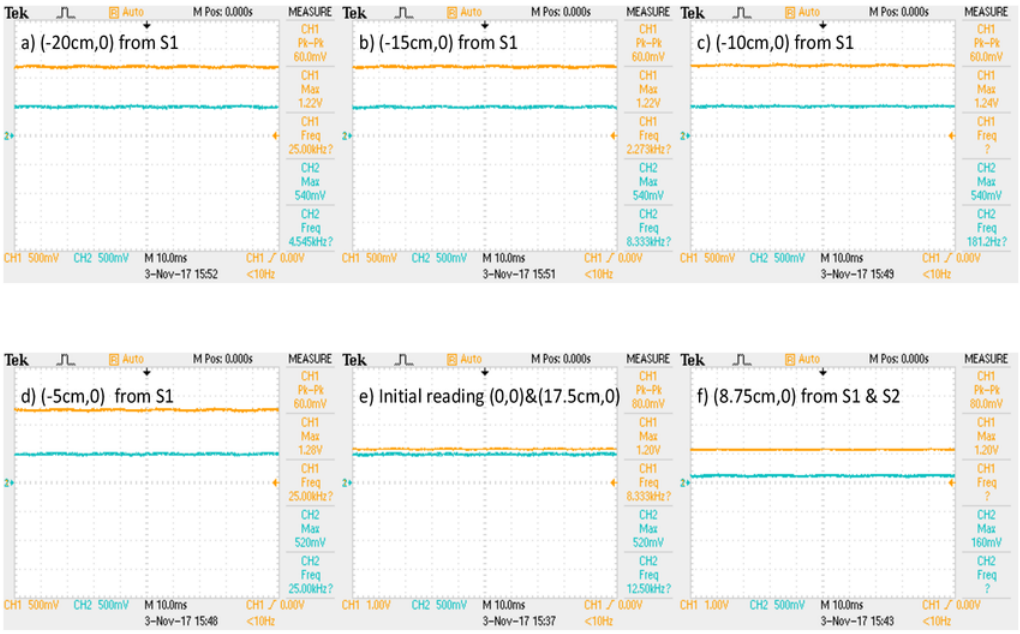

Figure A.6: *Oscilloscope recording as the meteorite sample is passed inline with the dual sensor setup.*

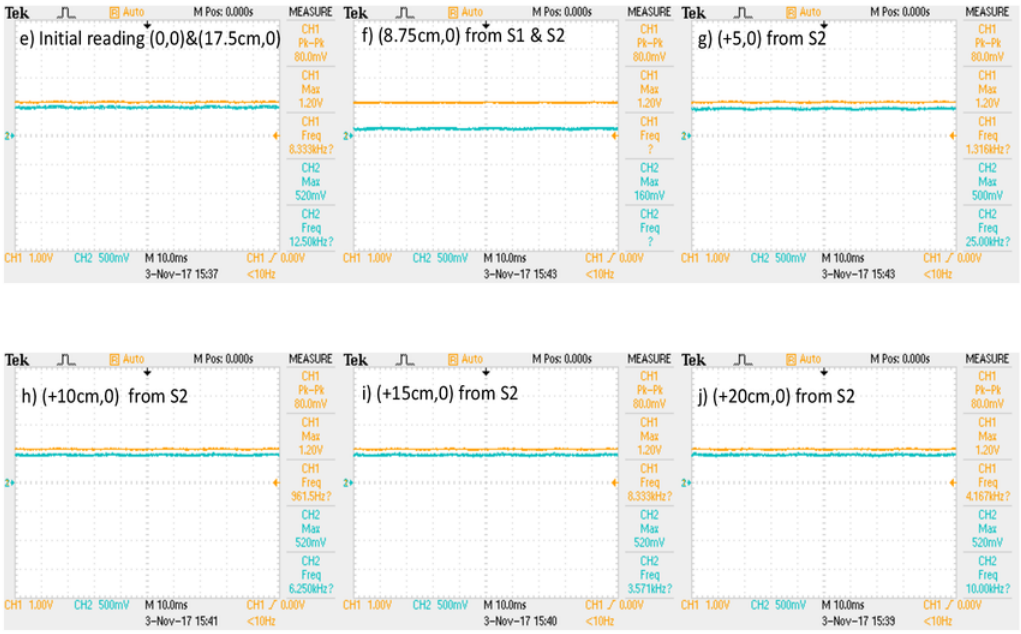

Figure A.7: *Oscilloscope recording as the meteorite sample is passed inline with the dual sensor setup.*

Bibliography

[1] D. S. Apostolopoulos, L. Pedersen, B. N. Shamah, K. Shillcutt, M. D. Wagner, and W. L. Whittaker, "Robotic antarctic meteorite search: Outcomes," in *Robotics and Automation, 2001. Proceedings 2001 ICRA. IEEE International Conference on*, vol. 4. IEEE, 2001, pp. 4174–4179.

[2] Arduino, "Arduino uno rev3," Website, 2017. [Online]. Available: https://store.arduino.cc/usa/arduino-uno-rev3

[3] A. Bevan, "Meteorites recovered from australia," *Journal of the Royal Society of Western Australia*, vol. 79, no. 1, pp. 33–42, 1996.

[4] ——, "Australian meteorites," *Records of the Australian Museum Supplement*, vol. 15, pp. 1–27, 1992.

[5] A. Bevan and R. Binns, "Meteorites from the nullarbor region, western australia: I. a review of past recoveries and a procedure for naming new finds," *Meteoritics & Planetary Science*, vol. 24, no. 3, pp. 127–133, 1989.

[6] B. Brown, "Ina 125 instrumentation amplifier with precision voltage reference," PDF, February 1998. [Online]. Available: http://www.ti.com/lit/ds/symlink/ina125.pdf

[7] M. Butta, "Orthogonal fluxgates," *High sensitivity magnetometers*, pp. 63–103, 2017.

[8] R. Citron, A. Shah, S. Sinha, C. Watkins, and P. Jenniskens, "Meteorite recovery using an autonomous drone and machine learning," in *Lunar and Planetary Science Conference*, vol. 48, 2017.

[9] J. ElkShoulder, O. Yawea, K. Gchachu, J. Simmons, B. Cohen, and H. Newsom, "Meteorite identification and classification using magnetic susceptibility. a." *Future*, vol. 1, p. 2, 1993.

[10] GeoscienceAustralia, "Australian geomagnetic reference field computation," Website, 2010. [Online]. Available: http://www.ga.gov.au/oracle/cgi/geoAGRF.sh?latd=-33&latm=46&lats=30&lond=151&lonm=06&lons=46&elev=0&year=2015&month=01&day=1&Ein=D&Ein=F&Ein=H&Ein=X&Ein=Y&Ein=Z&Ein=I

[11] A. Grosz, M. J. Haji-Sheikh, and S. C. Mukhopadhyay, *High sensitivity magnetometers*. Springer, 2017.

[12] T. Instruments, "ua741 general-purpose operational amplifiers," PDF, May 2017. [Online]. Available: http://www.ti.com/lit/ds/symlink/ina125.pdf

[13] Z. Instruments, "Sm30, shirt pocket – size magnetic susceptibility meter," ZH Instruments, Tech. Rep., 2016.

[14] M. Janosek, "Parallel fluxgate magnetometers," *High sensitivity magnetometers*, pp. 41–58, 2017.

[15] KeithleyInstrumentsInc, "Low level measurements handbook- 7th edition precision dc current, voltage, and resistance measurementsth edition," *Keithley*, 2016.

[16] Latitude.to, "Gps coordinates of macquarie university, australia," Website, 2017. [Online]. Available: http://latitude.to/articles-by-country/au/australia/5338/macquarie-university

[17] J. E. Lenz, "A review of magnetic sensors," *Proceedings of the IEEE*, vol. 78, no. 6, pp. 973–989, 1990.

[18] S. A. Macintyre, "Magnetic field measurement," in *Electrical Measurement, Signal Processing, and Displays*. CRC Press, 2003, pp. 12–46.

[19] S. Mayer, "Fluxgate magnetic field sensor fl1-500," PDF, 2017. [Online]. Available: http://www.lintronicstech.com/Fluxgate%20magnetic/Data%20sheet%20FL1-500.pdf

[20] ——, "Magnetic field sensor flc 100," PDF, 2017. [Online]. Available: http://www.stefan-mayer.com/images/datasheets/Data-sheet_FLC-100.pdf

[21] R. Moghimi, "Low noise signal conditioning for sensor-based circuits," *system*, pp. 1–16, 2010.

[22] D. Moorhouse, "Hyper-spectral imaging for airborne meteorite detection," 2014.

[23] C. Morón, C. Cabrera, A. Morón, A. García, and M. González, "Magnetic sensors based on amorphous ferromagnetic materials: A review," *Sensors*, vol. 15, no. 11, pp. 28 340–28 366, 2015.

[24] A. Orellana, "Low altitude drone assisted detection of meteorites in the australian desert," Undergraduate Research Report, 2016.

[25] L. J. Pesonen, M. Terho, and I. T. Kukkonen, "Physical properties of 368 meteorites: Implications for meteorite magnetism and planetary geophysics," *Antarctic Meteorite Research*, vol. 6, p. 401, 1993.

[26] PJRC, "Teensy usb development board," Website, 2016. [Online]. Available: https://www.pjrc.com/teensy/

[27] P. Ripka, *Magnetic Sensors and magnetometers*. Boston: Artech House, 2001.

[28] P. Rochette, J. Gattacceca, M. BOUROT-DENISE, G. Consolmagno, L. Folco, T. Kohout, L. Pesonen, and L. Sagnotti, "Magnetic classification of stony meteorites: 3. achondrites," *Meteoritics & Planetary Science*, vol. 44, no. 3, pp. 405–427, 2009.

[29] P. Rochette, J. Gattacceca, and M. Lewandowski, "Magnetic classification of meteorites and application to the soltmany fall," *Meteorites*, vol. 2, 2012.

[30] P. Rochette, L. Sagnotti, M. BOUROT-DENISE, G. Consolmagno, L. Folco, J. Gattacceca, M. L. Osete, and L. Pesonen, "Magnetic classification of stony meteorites: 1. ordinary chondrites," *Meteoritics & Planetary Science*, vol. 38, no. 2, pp. 251–268, 2003.

[31] A. Shah, C. Watkins, R. Citron, S. Sinha, and P. Jenniskens, "Meteorite discovery using unmanned aerial vehicles and convolutional neural networks," 2015.

[32] D. Tuite, "Understanding noise terms in electronic circuits," Website, March 2012.

[33] M. D. Wagner, D. Apostolopoulos, K. Shillcutt, B. Shamah, R. Simmons, and W. Whittaker, "The science autonomy system of the nomad robot," in *Robotics and Automation, 2001. Proceedings 2001 ICRA. IEEE International Conference on*, vol. 2. IEEE, 2001, pp. 1742–1749.